THE JOURNAL OF PHYSICAL CHEMISTRY A

Feature Article

Slow Electron Velocity-Map Imaging of Negative Ions: Applications to Spectroscopy and Dynamics

Daniel M. Neumark

J. Phys. Chem. A, **2008**, 112 (51), 13287-13301 • DOI: 10.1021/jp807182q • Publication Date (Web): 26 November 2008

CENTENNIAL FEATURE ARTICLE

Slow Electron Velocity-Map Imaging of Negative Ions: Applications to Spectroscopy and Dynamics†

Daniel M. Neumark*

Department of Chemistry, University of California, Berkeley, California 94720, and Chemical Sciences Division, Lawrence Berkeley National Laboratory, Berkeley, California 94720

Received: August 12, 2008; Revised Manuscript Received: October 7, 2008

Anion photoelectron spectroscopy (PES) has become one of the most versatile techniques in chemical physics. This article briefly reviews the history of anion PES and some of its applications. It describes efforts to improve the resolution of this technique, including anion zero electron kinetic energy (ZEKE) and the recently developed method of slow electron velocity-map imaging (SEVI). Applications of SEVI to studies of vibronic coupling in open-shell systems and the spectroscopy of prereactive van der Waals complexes are then discussed.

I. Introduction

Since its first implementation in 1967,[1] anion photoelectron spectroscopy (PES) has evolved into a highly versatile technique capable of addressing fundamental problems in spectroscopy and chemical dynamics. In PES, outlined schematically in Figure 1, mass selected negative ions are photodetached with a fixed-frequency light source, typically a pulsed or intense cw laser, and the resulting kinetic energy and angular distribution of the ejected photoelectrons are measured:

$$ABC^- \xrightarrow{h\nu} ABC + e^- \quad (1)$$

The neutral species ABC can be any species with a positive electron affinity, including some closed shell molecules and most free radicals. The PE spectrum then yields the electron affinity of ABC, the energetics of those excited electronic states that are accessible at the photodetachment energy, and, in favorable cases, vibrational frequencies for the active vibrational modes in each observed electronic state. The intensity progressions in these modes probe changes in geometry between the anion and neutral electronic states.

Since the anions are mass-selected prior to photodetachment, anion PES has proved extremely useful in elucidating energetic and spectroscopic trends in studies of size-selected clusters, where, for example, it can be used to probe the electronic states of a neutral metal cluster as a function of the number of constituent atoms, mapping out the evolution of electronic structure from the atomic to bulk limits.[2−8] Alternatively, one can study the energetic and spectroscopic effects of stepwise solvation of anions ranging from atomic halides to biomolecules,[9−12] and the solvation of electrons by water,[13−15] ammonia,[16,17] and other solvent molecules.[18,19] The species ABC does not have to be a stable species at all and, in fact, can be a transition state for a bimolecular or unimolecular chemical reaction. In such a case PES provides a means of carrying out "transition state spectroscopy", yielding vibrational levels of this elusive species, which is of central importance to much of chemistry.[20,21] Finally, the anion can have multiple negative charges, enabling gas phase studies of the multiply charged anions that play a key role in aqueous solution chemistry.[22]

A key factor in the versatility of anion PES is its relative simplicity; the information described above can generally be obtained at a single or at most a small number of detachment wavelengths. Hence, the photoelectron spectrum of any negative ion can, in principle, be measured with a reasonably simple laser system. However, this simplicity comes at a cost in energy resolution, which is determined not by the light source but the method used to analyze the electron kinetic energy distribution. This resolution is typically limited to 5−10 meV and can be much poorer. At this level of resolution, one can resolve vibrational and electronic fine structure in small molecules with a relatively sparse manifold of vibrational levels, but in species such as metal or semiconductor clusters, where there are typically numerous low-frequency vibrational modes, vibrational structure can be resolved only in favorable cases. When only electronic structure is resolved in cluster photoelectron spectra, one can infer structural information through comparison with electronic structure calculations, but there is considerably more ambiguity in the interpretation of the spectrum.

These considerations have driven efforts to develop photodetachment experiments that offer better resolution than PES while retaining as much of its flexibility and versatility as possible. One such method is anion zero electron kinetic energy (ZEKE) spectroscopy,[23] based on the analogous method developed for neutral species in the mid 1980s.[24,25] In anion ZEKE spectroscopy, as indicated in Figure 1, anions are detached with a tunable laser, and only those electrons produced with nearly zero kinetic energy are detected. Anion ZEKE indeed offers energy resolution as high as 0.1−0.2 meV, considerably better

† 2008 marked the Centennial of the American Chemical Society's Division of Physical Chemistry. To celebrate and to highlight the field of physical chemistry from both historical and future perspectives, *The Journal of Physical Chemistry* is publishing a special series of Centennial Feature Articles. These articles are invited contributions from current and former officers and members of the Physical Chemistry Division Executive Committee and from *J. Phys. Chem.* Senior Editors.

* To whom correspondence should be addressed. E-mail: dneumark@berkeley.edu.

10.1021/jp807182q CCC: $40.75
Published on Web 11/26/2008

Daniel M. Neumark is currently Professor of Chemistry at the University of California, Berkeley and has been Director of the Chemical Sciences Division at Lawrence Berkeley National Laboratory since 2000. He earned a B.A. and an M.A. from Harvard University in 1977 and a Ph.D. in Physical Chemistry from the University of California, Berkeley in 1984. His research focuses on chemical dynamics, spectroscopy, and cluster science, with particular emphasis on using negative ion photodetachment to probe transition states, radicals, and other transient species. More recent interests include developing femtosecond and attosecond light sources in the vacuum ultraviolet and soft X-ray regimes to probe novel aspects of chemical reaction and cluster dynamics.

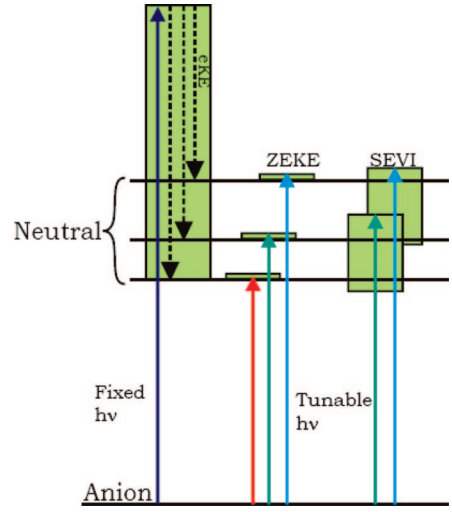

Figure 1. Comparison of anion photoelectron spectroscopy (left), zero electron kinetic energy (ZEKE) spectroscopy (center), and slow electron velocity-map imaging (SEVI, right).

than PES, and has been used to study small molecular species, clusters, and one transition state.[26] However, as discussed in the following section, it is experimentally quite challenging. Moreover, owing to the fundamental physics of negative ion photodetachment,[27] it is applicable only to a relatively small subset of negative ions.

Recently, we have developed a somewhat different approach to this problem based on a photoelectron imaging technique, slow electron velocity-map imaging (SEVI),[28] which offers photoelectron energy resolution comparable to that of anion ZEKE while retaining much of the versatility of PES. In SEVI, as indicated in Figure 1, one collects photoelectrons over a relatively narrow energy range at a discrete number of detachment wavelengths. In this sense, it is a hybrid between PES, where all electrons produced at a single wavelength are detected, and ZEKE, in which only near-zero energy electrons are detected as a function of a continuously tunable photodetachment wavelength. In SEVI, one essentially obtains a series of high resolution photoelectron spectra, each over a restricted energy range (typically 50−100 meV), that can be pieced together to generate a complete spectrum. In the relatively short time that has elapsed since SEVI was first introduced, it has been applied to a series of free radicals, clusters, prereactive van der Waals complexes, and reaction transition states.

In the following sections, the experimental principles and methodologies underlying anion PES, ZEKE, and SEVI are reviewed in more detail, with particular focus on the implementation and capabilities of SEVI. Several published and preliminary SEVI spectra are presented to illustrate its versatility and potential.

II. Review of Experimental Methods

A. Brief Review of Anion Photoelectron Spectroscopy. Anion photoelectron spectroscopy has its roots in the photoelectron spectroscopy of neutral species,[29,30] which was originally done using the vacuum ultraviolet light from discharge lamps or synchrotrons. Nearly all the electron energy analysis schemes used in anion experiments are adapted from methods developed for neutrals. In experiments on negative ions, target number densities are typically less than $10^6/cm^3$, many orders of magnitude lower than in experiments on neutral gas phase species. On the other hand, most anions can be photodetached at photon energies of 5 eV or less, allowing one to use intense visible or ultraviolet lasers that compensate for the lower target densities.

Anion photoelectron spectroscopy experiments were originally performed using a intracavity, cw Ar ion lasers to photodetach the ions and a hemispherical energy analyzer to determine the electron kinetic energy distribution.[1,31−33] This technology was perfected over many years in the laboratories of Lineberger,[34,35] Hotop,[36] and others,[37−39] yielding an electron kinetic energy (eKE) resolution as high as 5 meV. This experimental configuration is very versatile and can be combined with ion sources such as hot discharges, sputter sources, and flowing afterglows, enabling studies of a wide variety of negative ions. Indeed, far more small molecule electron affinities have been determined using this methodology than any other.[40] Its primary limitation is the maximum photon energy that can be reached with an intracavity Ar^+ laser, which is determined by the available transitions in the lasing medium; as of yet, 3.5 eV is the maximum photon energy at which PE spectra have been obtained with this configuration.[41]

In these experiments, the photoelectron angular distribution (PAD) can also be determined at each eKE by measuring the photoelectron intensity as a function of the angle θ between the electric field vector of the laser and the detection axis of the hemispherical analyzer. For single-photon detachment,[42] the PAD is given by

$$I(\theta) = \frac{\sigma}{4\pi}(1 + \beta P_2(\cos\theta)) \qquad (2)$$

where σ is the photodetachment cross section and β, the anisotropy parameter, varies from −1 to 2. The PAD and anisotropy parameter reflect the coherent superposition of partial waves of orbital angular momentum l produced by photodetachment. The anisotropy parameter is sensitive to the symmetry of the atomic or molecular orbital from which detachment occurs and to the final state produced by photodetachment.[43] While it is difficult to predict the value of β from first principles, its measurement can disentangle overlapping electronic bands and discern the presence of vibronic coupling between neutral electronic states.

In the 1980s, the development of pulsed ion sources and the desire to extend anion photoelectron spectroscopy further into the ultraviolet motivated a new generation of spectrometers based on pulsed laser photodetachment.[44] In these instruments, the first example of which was demonstrated by Johnson and co-workers,[45] anions are mass-selected by time-of-flight (TOF), ions of the desired mass are detached using a pulsed laser, and the resulting photoelectrons are energy-analyzed in a second TOF system. The anion sources typically involve pulsed molecular beam valves coupled to an electron gun,[46] an electric discharge,[47] or a laser-vaporization setup,[3,48] depending on whether gas phase or solid precursors are being used. The photodetachment wavelength can be a harmonic of a Nd:YAG laser, with harmonics up to the fifth harmonic (213 nm, 5.82 eV)[49] easily accessible via nonlinear frequency-doubling and mixing schemes, or an excimer laser wavelength which can be as low as 157 nm (7.8 eV).[50] Very recently, anion photoelectron spectra have been reported using the ninth harmonic of a Nd:YAG laser at 118 nm (10.8 eV).[51]

Both field-free and magnetic-bottle TOF analyzers have been extensively used to analyze the electron kinetic energy distribution. In field-free TOF,[45,49] photodetachment occurs in a magnetically shielded region and a small fraction of the photoelectrons are detected by a microchannel plate (MCP) detector lying 50−100 cm from the interaction region. In a magnetic bottle, an inhomogeneous magnetic field directs the photoelectrons ejected over a wide angular range to a MCP detector.[52,53] The field-free arrangement offers lower collection efficiency but higher resolution, as good as 5−10 meV. The resolution of the magnetic bottle suffers from severe Doppler broadening effects for ion beams in the keV range (a typical value in a TOF mass spectrometer),[54] but several laboratories have achieved resolution in the 10−40 meV range by slowing the ion beam or electrons in the laser interaction region.[55−58]

Another, more recent approach to anion photoelectron spectroscopy, pioneered by Bordas,[59,60] Sanov,[61,62] and their co-workers, makes use of photoelectron velocity-map imaging to detect and analyze the photoelectrons. These experiments build upon the photofragment and photoelectron imaging studies first carried out by Chandler[63,64] and Helm,[65] respectively, and the discovery of velocity-map imaging (VMI) by Parker and co-workers,[66] which greatly improved the energy resolution of both photoion and photoelectron imaging, resulting in the widespread use of both techniques in frequency and time-domain experiments.[67−72]

In anion photoelectron imaging, the ions are photodetached in a DC field of several hundred V/cm and the electrons are accelerated toward a MCP detector coupled to a phosphor screen. The resulting image of the photoelectrons is recorded by a CCD camera. The image is the projection of the photoelectron three-dimensional velocity distribution onto a two-dimensional plane; the original 3-D distribution can be recovered using well-established methods, thus yielding the photoelectron kinetic energy and angular distribution. Photoelectron imaging offers high collection efficiency with a typical energy resolution of 2−5%, although Cavanagh et al.[73] have improved on this considerably. In the usual mode of operation, where the DC fields are high enough to collect all the photoelectrons, 2−5% energy resolution is not very high, i.e., 20−50 meV for an electron kinetic energy of 1 eV. However, as detailed later in this section, the absolute energy resolution can be very high if one focuses only on the slow electrons; this is the basis of SEVI.

B. Anion ZEKE Spectroscopy. Experiments on neutral molecules by Schlag and Muller-Dethlefs[24,25] in the 1980s showed that one could improve on the resolution of photoelectron spectroscopy dramatically using a new technique, zero electron kinetic energy (ZEKE) spectroscopy. This work motivated the development of the analogous anion experiment in our laboratory[23,26] and elsewhere.[74−76] In anion ZEKE spectroscopy, mass-selected anions are photodetached with a tunable pulsed laser, and only those electrons with nearly zero kinetic energy are collected as the laser is scanned. The near ZEKE and higher energy electrons are allowed to separate spatially for ∼200 ns after the laser pulse fires, after which a weak pulsed electric field is applied to extract and detect the slow electrons; selective detection of the ZEKE electrons is achieved by a combination of spatial and temporal filtering.

ZEKE signal is seen when the laser passes through a photodetachment threshold between an anion and neutral level. Because only a very small range of kinetic energies (shaded areas in Figure 1) is collected at each laser wavelength, many small energy steps are required to record a full spectrum. The energy resolution can be as high as 1 cm^{-1}, but ZEKE spectra of most molecular anions have features at least 8−10 cm^{-1} wide owing to unresolved rotational structure.[77]

The physics of anion ZEKE are quite different than in neutral ZEKE experiments, which are now understood to involve pulsed field ionization of very high Rydberg states.[78,79] The near-zero energy electrons produced in the anion experiments are extremely sensitive to stray electric and magnetic fields, making these experiments quite difficult. In addition to the experimental difficulties, anion ZEKE spectroscopy is further complicated by the Wigner threshold law[80] which predicts the photodetachment cross-section σ to be

$$\sigma \propto (h\nu - E_{th})^{l+1/2} \quad (3)$$

where $h\nu - E_{th}$ is the energy difference between the photodetachment laser and detachment threshold, and l is the angular momentum of the photoelectron. Clearly, σ is always zero at threshold and increases rapidly with photon energy only if l is zero (s-wave scatterers). For all systems with $l > 0$, σ remains close to zero for an energy range of several meV above threshold, thereby preventing the recording of a ZEKE spectrum.

The advantages and limitations of anion ZEKE spectroscopy are exemplified in Figure 2, which shows the anion photoelectron and ZEKE spectra of Si_4^-.[81,82] Electronic structure calculations predict both the anion and neutral are planar rhombus structures with D_{2d} symmetry.[83] The photoelectron spectrum at 355 nm shows two electronic bands, assigned to transitions to the $\tilde{X}^1A_g$ ground state (band X) and $\tilde{A}^3B_{3u}$ excited state (band A) of Si_4. Each band shows partially resolved vibrational structure with peak spacing of 360 (X) and 300 cm^{-1} (A), assigned in both cases to a progression in the ν_2 totally symmetric bending mode of Si_4. The anion ZEKE spectrum of band A shows considerably better resolution. The main progression in the ν_2 mode is fully resolved, and it is apparent that the spectrum exhibits substantial finer structure in addition to the main progression. These additional features surrounding each of the main peaks have been assigned to sequence and combination bands involving the low-frequency ν_3, ν_5, and ν_6 modes.

What about the ZEKE spectrum of band X? This band does not appear at all in the ZEKE spectrum, a result that reflects the limitations imposed by the Wigner threshold law. Si_4^- has a $^2B_{2g}$ ground-state with molecular orbital configuration...$(a_g)^2(b_{1u})^2(b_{2g})$. The $\tilde{X}^1A_g$ and $\tilde{A}^3B_{3u}$ neutral states are accessed by photodetachment from the b_{2g} and b_{1u} orbitals, respectively. The selection rules for photodetachment dictate that detachment from an orbital with

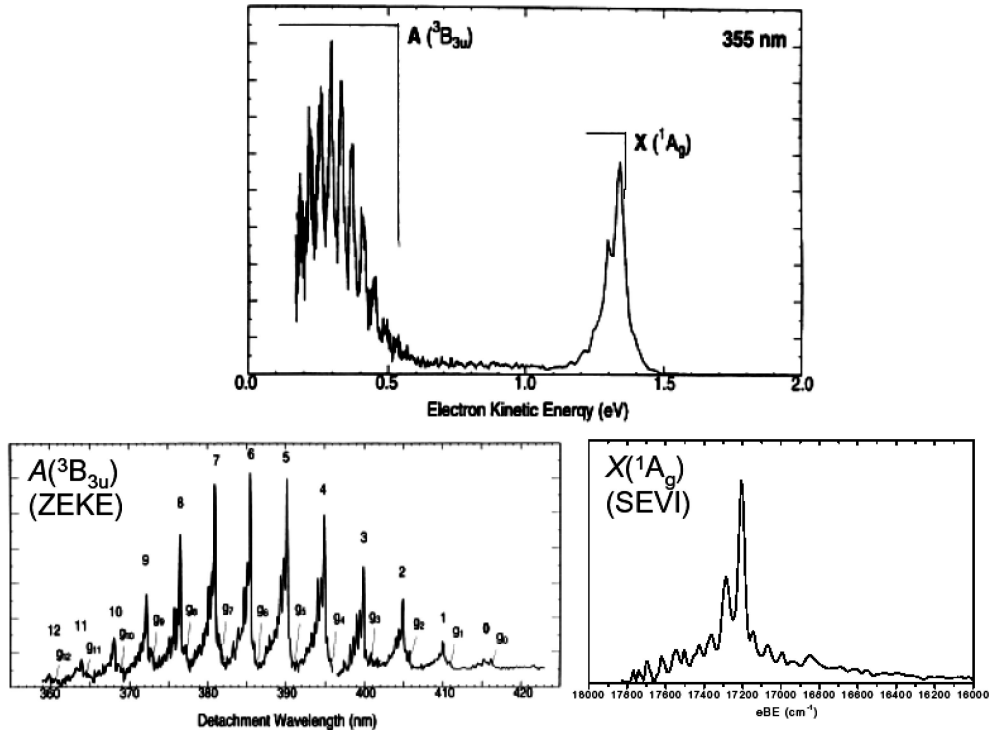

Figure 2. Comparison of photoelectron spectrum of Si_4^- at 355 nm (top left, ref 81), ZEKE spectrum of band A (bottom left, ref 82), and SEVI spectrum of band X (right).

gerade symmetry can only lead to odd partial waves for the detached electron.[84] Hence, photodetachment to the Si_4 ground-state will produce a *p*-wave electron, and, according to eq 3, this cross section will be very small near the detachment threshold. In contrast, photodetachment to the $\tilde{A}^3B_{3u}$ state involves removal of an *ungerade* electron and can proceed via *s*-wave production, resulting in a measurable ZEKE spectrum.

This issue regarding *s*-wave detachment is more troublesome than might appear at first glance. While the symmetry of the molecular orbital from which detachment occurs dictates whether *s*-wave production is allowed,[84] it is difficult to tell a priori how large the partial cross section for *s*-wave detachment is for a given species. We thus found that anion ZEKE worked very well for some classes of anions, including small carbon,[85,86] silicon,[82,87−89] and germanium[90,91] clusters and rare gas/halide complexes,[77,92,93] but many systems that could in principle detach via *s*-waves showed no appreciable ZEKE signal. Hence, the development of a high resolution photodetachment technique that is not so constrained by eq 3 is highly desirable. One such method, developed by Cheshnovsky,[94] achieves sub-meV resolution by detaching anions further above threshold than in ZEKE (i.e., a few meV), and only detecting electrons in a narrow kinetic energy window as the photodetachment laser is tuned. The idea of achieving high resolution while detaching above threshold also plays a central role in SEVI, as discussed in the following section.

C. Anion SEVI. SEVI is, in principle, a simple variant of photoelectron imaging. In SEVI, mass-selected anions are photodetached at a set wavelength. The resulting photoelectrons are collected via velocity-map imaging (VMI) using relatively low extraction voltages, with the goal of selectively detecting slow electrons with high efficiency and enlarging their image on the detector. A series of images is obtained at different wavelengths, each yielding a high resolution photoelectron spectrum over a limited range of electron kinetic energy. The basic ideas is that if the canonical 2% energy resolution of VMI can be achieved for electrons with 10 meV of kinetic energy, the absolute energy resolution is 0.2 meV (1.6 cm^{-1}). SEVI draws upon the photoionization and photodetachment microscopy experiments reported previously by Vrakking,[95] Blondel,[96,97] and co-workers; those experiments were more concerned with measuring interference effects associated with extremely slow electrons, rather than as a means of carrying out high resolution photoelectron spectroscopy over an extended energy range.

Figure 3 shows the current version of our SEVI instrument.[28,98] Anions are generated by expanding an appropriate gas mixture into the source vacuum chamber through an Even-Lavie pulsed valve equipped with a circular ionizer. Anions formed in the gas expansion are extracted into a Wiley−McLaren time-of-flight mass spectrometer and directed to the detachment region by a series of electrostatic lens and pinholes. A 1 μs pulse on the last ion deflector allowed only the desired mass into the interaction region. Anions are photodetached between the repeller and the extraction plates of a three-plate VMI electron optical stack by the focused output of a Nd:YAG pumped tunable dye-laser. Repeller voltages typically range from 150 − 350 V. The photoelectron cloud formed is coaxially extracted down a 50 cm flight tube and mapped onto a detector comprising a chevron-mounted pair of time-gated, imaging quality microchannel plates coupled to a phosphor screen, as is typically used in photofragment imaging experiments. Events on the screen are collected by a 1024 × 1024 Charge-Coupled Device (CCD) camera and sent to a computer. Electron velocity-mapped images resulting from 25 000−100 000 laser pulses are summed, quadrant symmetrized and inverse-Abel transformed.[99] Photoelectron spectra are obtained via angular integration of the transformed images.

In order to obtain circular images at these low extraction voltages, care must be taken to eliminate stray electric and magnetic fields in the photodetachment region and free-flight region. Both are enclosed within two concentric cylinders of magnetic shielding, the innermost surface of which is coated

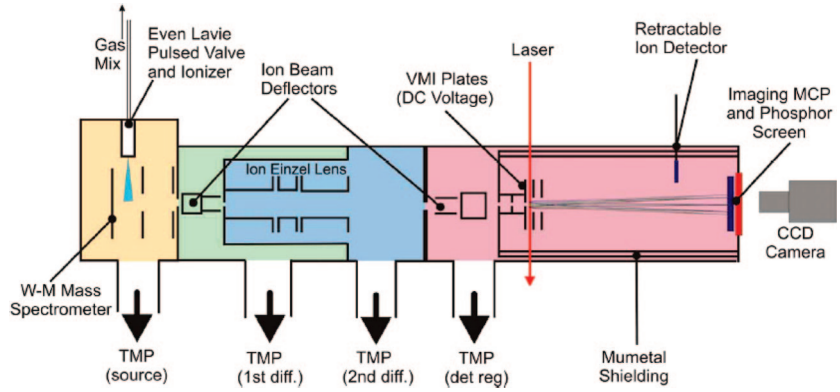

Figure 3. Schematic of SEVI apparatus.

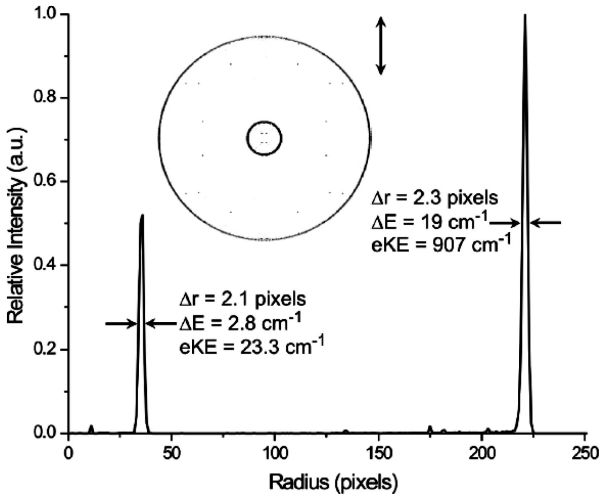

Figure 4. Transformed image of Cl^- (inset) showing photodetachment to $Cl(^2P_{3/2})$ (outer ring) and $Cl^*(^2P_{1/2})$ (inner ring). Angular integration yields photoelectron signal vs pixel position, as shown. Kinetic energies and linewidths for the two peaks are indicated (ref 98).

with colloidal graphite. The coaxial VMI arrangement is also important, as it eliminates any effects of the energy spread in the anion beam on the electron energy resolution.

Figure 4 shows the transformed SEVI image and angular integration of the photoelectron signal of the atomic chloride ion at a photodetachment wavelength of 332.9 nm and a repeller voltage of 350 V.[98] The outer and inner rings correspond to photodetachment to the $Cl(^2P_{3/2})$ ground-state and $Cl^*(^2P_{1/2})$ spin−orbit excited state, respectively. Both rings are about two pixels wide, but the corresponding energy widths ΔE, given by

$$\frac{\Delta E}{eKE} = 2\frac{\Delta r}{r} \tag{4}$$

are 2.8 and 19 cm^{-1} for the inner and outer rings, respectively, as shown in Figure 4. At repeller voltage of 150 V, the rings are larger and even higher resolution can be obtained; peaks as narrow as 1.5 cm^{-1} have been measured for the transition to the Cl* state, for example. One can also obtain PAD's from the images. The inner ring is nearly isotropic ($\beta = -0.1$), as expected for *s*-wave detachment near threshold. The outer ring is more anisotropic with $\beta = -0.3$, indicating that there is an additional contribution from *d*-wave detachment further above the threshold.

The energy resolution of SEVI is comparable to that of anion ZEKE, but SEVI offers considerable advantages. While a ZEKE spectrum requires stepping the photodetachment laser at small energy intervals, typically 0.3−1 cm^{-1}, a complete SEVI spectrum can be obtained using much larger intervals, typically 100−1000 cm^{-1}, and in favorable cases a single wavelength suffices. Moreover, in a given SEVI spectrum, the excess energy above threshold, $h\nu - E_{th}$, is typically much larger than in ZEKE where one is by necessity within 2−3 cm^{-1} above the photodetachment transition of interest. Hence, the photodetachment cross section is much higher in SEVI. These two effects combine to yield data collection rates approximately 2 orders of magnitude higher in SEVI. This difference also means that it is possible to observe *p*-wave detachment in SEVI; at photon energies 100−200 cm^{-1} above threshold, the cross section for *p*-wave detachment is no longer negligible. Thus, for example, the SEVI spectrum of band X can be measured, as shown in Figure 2, where we now observe an as yet unassigned progression with a peak spacing of 80 cm^{-1} that was not resolved in previous work.[81,100]

SEVI does have at least one disadvantage compared to energy-dispersive photoelectron analysis schemes in that a weak feature at low eKE can be obscured by a strong feature at high eKE, because the images from both features cover the same detector pixels. With sufficiently high signal-to-noise, one should be able to discern the weaker feature, but the dynamic range of the spectrometer is still limited. This constraint would disappear if the methodology of photofragment "slice" imaging[101,102] could be adapted to photoelectron imaging, but so far this has not proved feasible.

III. Applications of SEVI

The high spectral resolution afforded by SEVI provides the means to observe underlying structure that was not resolved in more conventional photoelectron spectroscopy experiments. This capability is critical in looking at species with numerous low-frequency vibrational modes, such as metal and semiconductor clusters, as exemplified in the case of Si_4 shown above. Moreover, at higher resolution, one can unravel vibronic coupling and other non-Born−Oppenheimer (BO) effects that often play an important role in the open-shell free radicals and clusters generated by photodetachment. The elucidation of these effects is a frontier area in photoelectron spectroscopy of both anions and neutrals.[103,104]

Allowed transitions involving progressions in totally symmetric vibrational modes can generally be simulated within the Franck−Condon (FC) approximation, in which the transition strength between the anion and neutral vibrational levels $|\Psi^-(v_1''...v_n'')\rangle$ and $|\Psi^0(v_1'...v_n')\rangle$, respectively, is given by

$$I \propto \left|\langle \Psi^-(v_1''....v_n'') \middle| \Psi^0(v_1'...v_n') \rangle\right|^2 \tag{5}$$

The multidimensional FC factor in eq 5 can be evaluated either by invoking the parallel mode approximation, in which

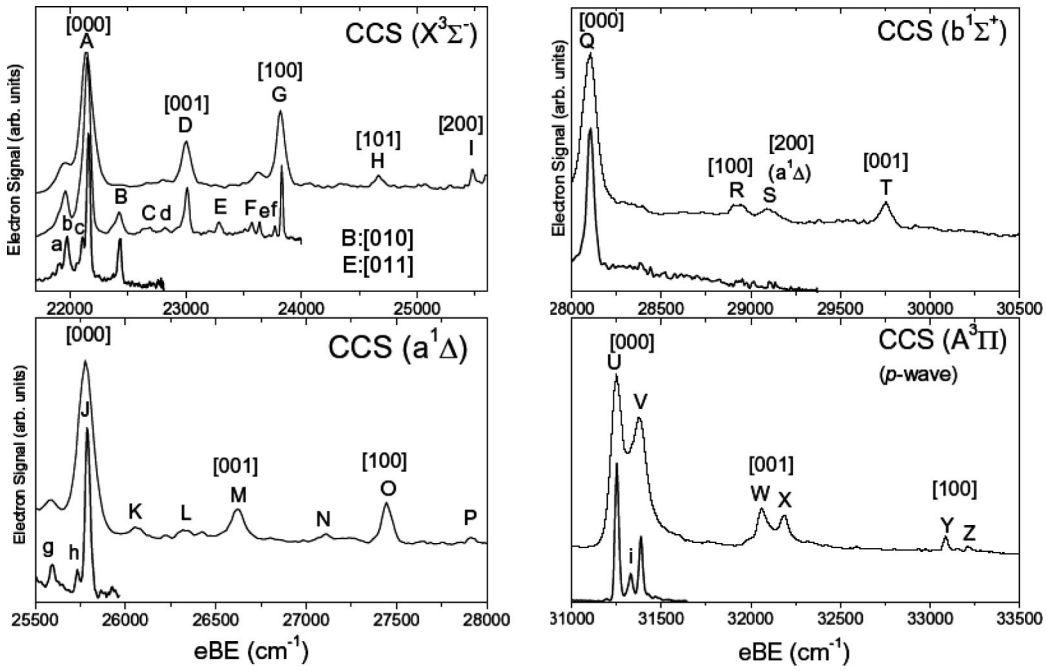

Figure 5. SEVI spectrum of CCS^-, showing transitions to the four lowest lying electronic states of CCS (ref 115). The lower curves in each panel were taken at a lower photodetachment energy, resulting in higher resolution over a narrower energy window.

case it breaks up into n one-dimensional FC factors, or allowing for Duschinsky mixing between modes of the same symmetry.[41,105] Any Δv transition in a totally symmetric mode is allowed, and $\Delta v = \pm 2, \pm 4, \ldots$ transitions in nontotally symmetric modes are also allowed but tend to be very weak compared to $\Delta v = 0$.

However, odd Δv transitions in nontotally symmetric modes can occur only through vibronic coupling effects, i.e. the breakdown of the Born−Oppenheimer approximation induced by the nuclear kinetic energy operator.[106] These effects include Renner−Teller (RT), Jahn−Teller (JT), and Herzberg−Teller (HT) coupling, all of which can introduce nominally forbidden transitions in photoelectron spectra. For example, in photodetachment transitions to degenerate electronic states, JT coupling can lead to progressions in degenerate vibrational modes of the neutral, as seen in the photoelectron spectrum of the $C_5H_5^-$ anion, where weak JT coupling in the $\tilde{X}^2E_1''$ ground-state of C_5H_5 results in a short progression in two of the e_2' degenerate stretching and bending modes.[107,108]

HT coupling mixes vibronic levels of the same overall symmetry nominally associated with two (or more) different electronic states and explains, for explain, the presence of $\Delta v_4 = 1$ transitions in the ground-state band of the photoelectron spectrum of NO_3^-.[109] The NO_3 radical has a $\tilde{X}^2A_2'$ ground state, and the ν_4 mode is an in-plane bend with e′ symmetry. The $v_4 = 1$ level thus has E′ vibronic symmetry, and can mix with totally symmetric vibrational levels of the $\tilde{B}^2E'$ electronic state of NO_3 that lies 1.88 eV above the ground state. This qualitative picture is supported by theoretical treatments of NO_3.[110−113] If allowed transitions to the two neutral electronic states have different PAD's, then transitions that acquire intensity through HT coupling can exhibit the PAD associated with the distant, vibronically coupled electronic state. Hence, the observation of a peak in the middle of a band with a different PAD from the rest of the band is a distinct signature of vibronic coupling, as seen in the photoelectron spectra of C_2H^- and BNB^-.[35,114]

A. Probing Vibronic Coupling in Free Radicals with SEVI. As an example of a fairly simple system, we have recently applied SEVI to CCO^- and CCS^-, species for which both the anion and neutral are linear.[115] The resulting spectra for each anion show transitions from the anion $^2\Pi$ state to the neutral $\tilde{X}^3\Sigma^-$ ground-state and low-lying $\tilde{a}^1\Delta$, $\tilde{b}^1\Sigma^+$, and $\tilde{A}^3\Pi$ states, in agreement with lower resolution PE spectra of CCO^-.[116,117]

The four bands for CCS^- photodetachment are shown in Figure 5. The spectra are plotted with respect to electron binding energy (eBE), the difference between the photon energy and the electron kinetic energy (eKE):

$$eBE = h\nu - eKE \tag{6}$$

The high energy termination point of each spectrum corresponds to the photon energy with which each image was acquired. The SEVI spectra are dominated by allowed transitions in the CCO and CCS stretching modes, and show fine-structure from spin−orbit splitting in the anion and, for CCS, the neutral $\tilde{A}^3\Pi$ state. There is no evidence for vibronic coupling in CCO, but in CCS, there is some bending activity in the $\tilde{X}^3\Sigma^-$ band, and nominally forbidden bend transitions (peaks B and E) have PAD's characteristic of the $\tilde{A}^3\Pi$ band, indicative of Herzberg−Teller coupling between these states.

The carbon monohydride radicals, $C_{2n}H$, exemplify the capabilities of SEVI to probe more complex vibronic coupling effects. These radicals are of interest in combustion[118] and have been identified in the interstellar medium,[119,120] along with some of the corresponding anions.[121,122] Microwave spectra[123,124] have shown that they are linear, at least up to $n = 7$. These radicals are of interest from the perspective of vibronic coupling because they have close-lying $^2\Sigma^+$ and $^2\Pi$ electronic states, whose spacing and energy-ordering depends on the length of the carbon chain. The most thoroughly studied member of this series is C_2H, for which the ground-state is $\tilde{X}^2\Sigma^+$ and the $\tilde{A}^2\Pi$ excited-state lies about 3700 cm^{-1} higher,[125] but the $^2\Pi$ state becomes progressively more stabilized for the longer chains. Both states are accessible by photodetachment from the $C_{2n}H^-$ anion, which has a linear $\tilde{X}^1\Sigma^+$ ground state, by detachment from either a σ or π molecular orbital, so photoelectron spectroscopy provides a direct means of determining the location and splitting of the two neutral states. Indeed, photoelectron spectra[126] of the series

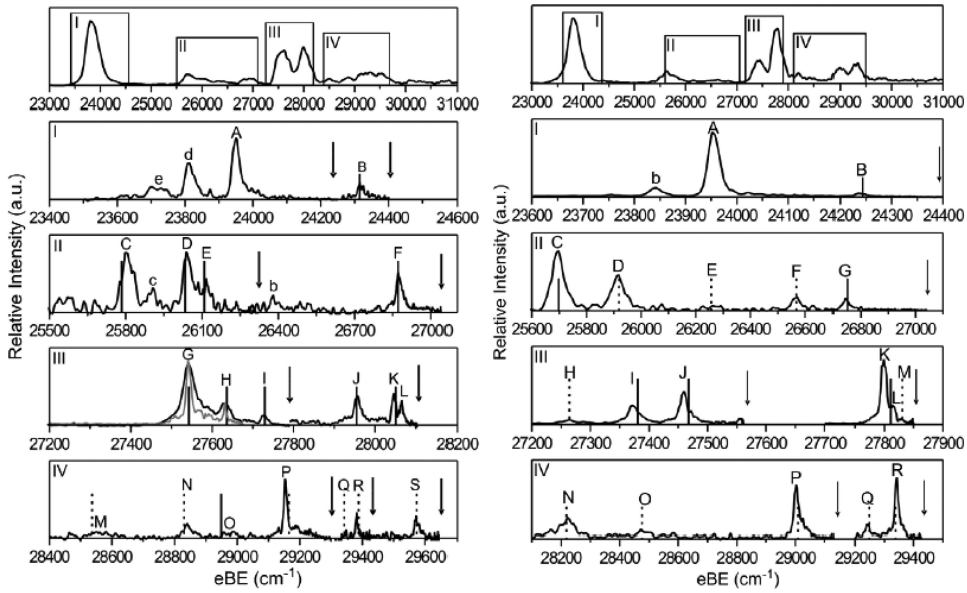

Figure 6. Left panels: PE spectrum of C_2H^- at 266 nm in top panel, and SEVI spectra of regions I−IV in lower four panels. Right panels: same, but for C_2D^- (ref 98).

C_2H^- to C_8H^- showed that the $^2\Sigma^+$ and $^2\Pi$ states are nearly degenerate in C_4H, with the $^2\Sigma^+$ state lying slightly lower, but that the $^2\Pi$ state is the ground-state for C_6H and C_8H. These assignments were made in part based on the observed photoelectron angular distributions, which quite different depending on the orbital from which detachment occurs; the measured PAD's indicate mainly *p*-wave detachment to the $^2\Sigma^+$ state and *s*-wave detachment to the $^2\Pi$ state.

We first consider the C_2H radical, which exhibits complex vibronic coupling in its ground-state owing to a conical intersection between the ground $\tilde{X}^2\Sigma^+(A')$ state and the low-lying $^2\Pi(A')$ and $^2\Pi(A'')$ states.[127,128] Along the linear axis, there is Renner-Teller coupling between the electronic and vibrational angular momenta of the $^2A'$ and $^2A''$ components of the $^2\Pi$ state, while the bend vibration induces pseudo Jahn−Teller (aka Herzberg−Teller) coupling between the $^2\Sigma^+$ state and the $^2A'$ component of the $^2\Pi$ state. The resulting breakdown of the Born−Oppenheimer approximation complicates vibrational assignments of the C_2H radical, and poses a challenge to both theory and experiment.

Much of our understanding of these effects in C_2H has come from rotationally resolved IR spectroscopy,[125,129] but PE spectroscopy of C_2H^- has provided additional and complementary information. Ervin et al.[35] measured the first photoelectron spectra of C_2H^- and C_2D^- at a photon energy of 3.52 eV. They observed a spectrum dominated by the $\tilde{X}^2\Sigma^+-\tilde{X}^1\Sigma^+$ 0−0 origin band, indicating a small geometry change between the anion and the radical ground state. The PE spectrum exhibited numerous transitions involving the bending (υ_2) and the C−C stretching (υ_3) modes. The observation of odd $\Delta\upsilon_2$ transitions with a different PAD than the allowed transitions in this band implied HT coupling with the $\tilde{A}^2\Pi$ state.

In the higher energy PE spectra (4.66 eV) of C_2H^- and C_2D^- reported by Taylor et al.,[126] strong transitions were observed in the region of the $\tilde{A}^2\Pi$ state origin, where overlapped transitions to the $\tilde{X}^2\Sigma^+$ and $\tilde{A}^2\Pi$ states were expected. Assignments were made based on previous experiments and the photoelectron angular distributions, based on the reasoning that transitions to neutral levels with dominant $\tilde{A}^2\Pi$ state character would show different angular distributions than those primarily associated with the $\tilde{X}^2\Sigma^+$ state. Nonetheless, some of the assignments were problematic. Hence, SEVI spectra at higher resolution were needed to determine the extent to which overlapping transitions contributed to the PE spectrum, and to obtain improved assignments.

Figure 6 shows the PE spectra of C_2H^- and C_2D^- measured by Taylor et al. in the top panels, while the lower panels show SEVI spectra of selected regions of the PE spectra.[98] The SEVI spectra indeed show that nearly all features in the PE spectra comprise multiple transitions, and that most of these transitions can be assigned by comparison to prior experiment or theory[128] (solid and dashed lines, respectively). Region III is the most interesting, since it is where the origin of the $\tilde{A}^2\Pi$ state is expected. The two peaks in this region of the C_2H^- PE spectra split into six features in the SEVI spectrum. These features are assigned to transitions from the anion ground-state to neutral states that are admixtures of the ground vibrational level of the $\tilde{A}^2\Pi$ state, the $\tilde{A}(000)$ level, with various vibrational levels of the $\tilde{X}^2\Sigma^+$with odd numbers of quanta in the υ_2 bending mode. The states comprising each admixture have overall Π vibronic symmetry. In the absence of vibronic coupling, there would be a single feature corresponding to a transition to the $\tilde{A}(000)$ state, but vibronic coupling spreads the oscillator strength for the transition over several nearby levels with the same vibronic symmetry. For C_2D^-, the SEVI spectrum of region III is considerably simpler, reflecting reduced vibronic coupling in the C_2D radical;[125,130] feature K has considerably more $\tilde{A}(000)$ character than any of the nearby peaks and consequently dominates the SEVI spectrum.

SEVI spectra of C_4H- are presented in Figure 7.[131] In this figure, one observes that as the laser frequency is lowered, fewer features are observed but the resolution improves, as expected based on eq 4. Five well-separated bands are present, corresponding to the partially resolved features in the previously recorded PE spectra.[126] The higher resolution spectra in reveal that several of the bands are doublets with splittings ranging from 15−35 cm^{-1}, and there are several additional minor peaks as well.

PAD's for closely spaced features are markedly different, as can be seen directly from the photoelectron image in Figure 7, the SEVI image corresponding to the bottom photoelectron spectrum. The two rings corresponding to features B and C are

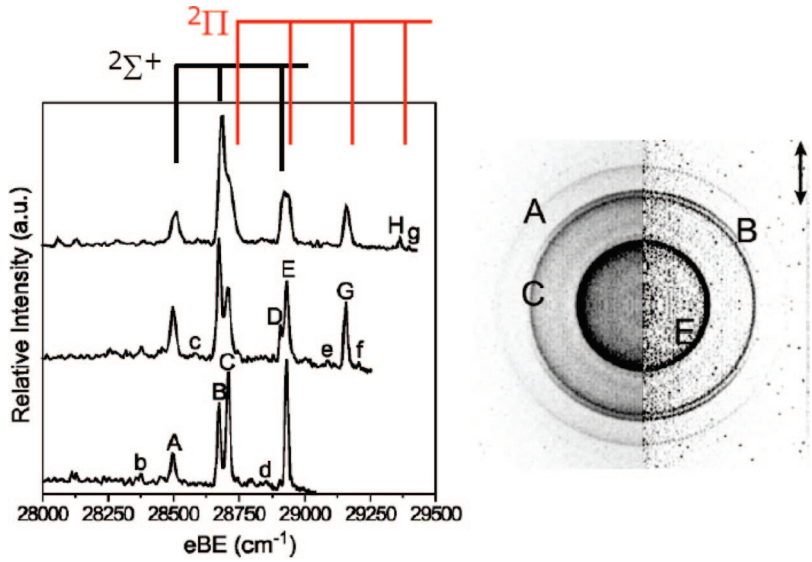

Figure 7. Left: SEVI spectra of C_4H^- at various photon energies. Right: SEVI image of C_4H- corresponding to bottom spectrum (ref 131).

clearly distinguished, and while C is isotropic, B is strongly peaked along the direction of laser polarization. Peaks A, B, and D exhibit PAD's characteristic of *p*-wave scattering, while the remaining main features in the spectrum, peaks C, E, F, G, and H, exhibit *s*-wave PAD's. The nature of the photoelectron partial waves is also consistent with the dependence of peak intensities upon photon energy. According to eq 3, transitions dominated by *p*-wave detachment will drop more quickly than those dominated by *s*-wave detachment as the photon energy is lowered, and that is exactly what is seen in Figure 7.

It thus appears that the SEVI spectrum comprises two overlapping transitions to two different electronic states of C_4H, a result consistent with past theoretical[132,133] and experimental[126] work indicating that the $^2\Sigma^+$ and $^2\Pi$ are very close to one another. Based on the PAD's, peaks A and C are assigned to the vibrational origins of the $\tilde{X}^2\Sigma^+$and $\tilde{A}^2\Pi$ states, respectively, yielding a splitting of only 26 meV (213 cm^{-1}) between the states. This splitting is close to the most recent calculated value, 35 meV,[134] and represents an improvement over the previously reported value of 468 cm^{-1} inferred from our lower resolution PE spectrum[126] where it was more difficult to identify the band origins.

Similarly, peaks B and D are assigned to transitions within the $\tilde{X}^2\Sigma^+$ manifold, while the remaining peaks are assigned to transitions within the $\tilde{A}^2\Pi$ manifold. Peak spacings in the vibrational progressions are around 200 cm^{-1}, which is too low to be anything other than a bending mode of C_4H, and all observed features can be assigned to transitions in the degenerate ν_6 and ν_7 bending modes are based primarily on comparison to electronic structure calculations. However, the presence, let alone the dominance, of activity in the bending modes is unusual considering that the anion and both neutral states are linear. We therefore must consider effects from HT coupling, which mixes close-lying levels of the same vibronic symmetry that are nominally associated with different electronic states. Thus, odd levels of bend modes of the $\tilde{X}^2\Sigma^+$ state, with overall Π vibronic symmetry, mix with even levels of bend modes of the $\tilde{A}^2\Pi$ state with the same vibronic symmetry, and transitions from the anion ground-state to these levels become allowed. Similarly, odd bending levels of the~$\tilde{A}^2\Pi$ state with Σ^+ symmetry mix with Σ^+ levels of the $\tilde{X}^2\Sigma^+$ state and become accessible to detachment from the anion ground state. The SEVI spectra, which show strong odd $\Delta\nu$ transitions in the bending modes of both the $\tilde{X}^2\Sigma^+$ and $\tilde{A}^2\Pi$ states, can be explained within the context of this type of coupling, and given that the electronic state splitting is comparable to the frequency of the relevant vibrational modes, strong HT coupling is certainly expected in C_4H.

Other examples in which SEVI has been used to probe vibronic coupling include studies of the propynyl anion, H_3CCC^-,[135] and the methoxide[136] and ethoxide anions. The SEVI spectrum of H_3CCC^- provides a reasonably high resolution probe of vibronic structure in the propynyl radical, H_3CCC. The propynyl radical is a higher energy isomer of the propargyl radical, H_2CCCH; recent calculations place it about 40 kcal/mol above propargyl.[137,138] Thus, while many experimental studies of propargyl have been reported,[139] propynyl has been quite difficult to isolate and study spectroscopically; its only prior experimental characterization came from the anion PE spectrum measured by Robinson et al.[140] Propynyl has C_{3v} symmetry and electronic structure calculations have indicated it has a $\tilde{X}^2A_1$ ground-state and a low-lying $\tilde{A}^2E$ excited state.[141] Thus, transitions from the anion to $\tilde{X}$ state vibrational levels with *e* symmetry can only occur via vibronic coupling with the $\tilde{A}^2E$ state.

The SEVI spectrum of H_3CCC^- is shown in the lower two panels of Figure 8,[135] along with the previously measured photoelectron spectrum[140] in the top panel. Peak A, the dominant spectral feature, is the band origin of the transition to the $\tilde{X}^2A_1$ state. High resolution scans of this feature (inset, bottom panel) show a partially resolved triplet of peaks spaced by 5−6 cm^{-1} that are assigned to rotational contours associated with parallel ($\Delta K = 0$) and perpendicular ($\Delta K = \pm 1$) transitions. The much smaller features to the left of peak A are assigned to sequence bands in the low frequency degenerate C−C−C bend mode (the ν_8 mode), while nearly all the remain features to the right of peak A can be assigned to transitions to totally symmetric vibrational levels of the $\tilde{X}^2A_1$ state, with the exception of the weak peak I, which is attributed to the vibrational origin of the $\tilde{A}^2E$ state. No vibronic coupling needs to be invoked to explain the spectrum. The absence of observable coupling is somewhat surprising, given the proximity of the two electronic states, but may reflect the low photodetachment cross section to the $\tilde{A}^2E$ state, in which case "intensity-borrowing" will not provide much enhancement of nominally forbidden transitions within the $\tilde{X}^2A_1$ sate manifold.

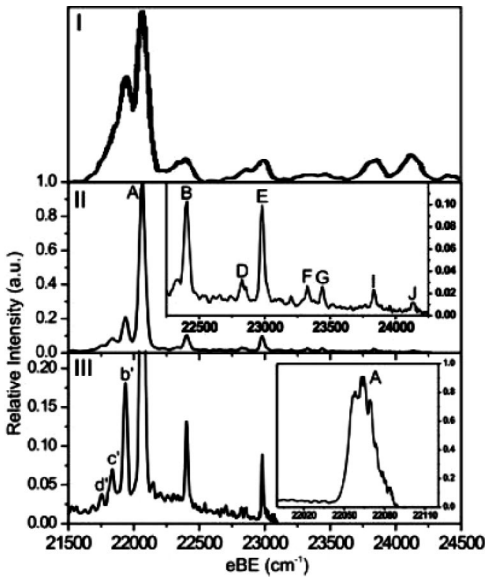

Figure 8. Comparison of photoelectron spectrum (top) of propynyl anion (H_3CCC^-) from ref 140 and SEVI spectra (ref 135;) in bottom two panels. Panel III was taken at a photodetachment energy closer to the band origin (peak A) to obtain higher resolution. The inset in panel III was taken just above the band origin and shows partially resolved rotational contours.

The methoxy (CH_3O) and ethoxy (C_2H_5O) radicals are particularly interesting species from the perspective of probing vibronic coupling via various photodetachment spectroscopies. The CH_3O radical has C_{3v} symmetry. Its $\tilde{X}^2E$ ground state, with a half-filled *p*-orbital on the O atom, has been a model system for exploring the effects of Jahn−Teller coupling through a combination of laser-induced fluorescence,[142−145] dispersed fluorescence,[146−148] stimulated emission pumping,[149,150] photoelectron spectroscopy,[151−153] photodissociation,[154,155] and several theoretical studies.[156−159] The effects of Jahn−Teller coupling in CH_3O are particularly pronounced in the photoelectron spectrum[152,153] CH_3O^-. These spectra, all of which involve photodetachment to the $\tilde{X}^2E$ state of CH_3O, show various degrees of vibrational and spin−orbit fine structure, depending on their resolution, but they are unusual in that they are dominated by progressions in the ν_5 and ν_6 e′ degenerate vibrational modes, a clear manifestation of Jahn−Teller coupling in the methoxy ground state. The SEVI spectrum[160] of CH_3O^- resolves these progressions more clearly, as well as spin−orbit fine structure and additional weak vibrational features. Most of the features in the PE and SEVI spectra can be assigned, even if simulation of the spectral intensities is still problematic.

The ethoxy radical presents a more challenging scenario. C_2H_5O also has an unpaired electron on the O atom, but owing to its lower (C_s) symmetry, the degeneracy seen in CH_3O is removed, leading to a ground $\tilde{X}^2A''$ state and low-lying $\tilde{A}^2A'$ state.[161,162] The anion PE spectrum measured by Ramond et al.,[153] shown in the left panel of Figure 9, shows that the $\tilde{X}^2A''$ and $\tilde{A}^2A'$ states are separated by only 355 cm^{-1}; the band origins for the two states, peaks a and b, respectively, were identified through their very different PAD's. The remainder of the spectrum is quite congested, however, as it comprises overlapped transitions to the two electronic states. The PAD's were used to attribute these features to one state or the other, but only a single vibrational progression in the ground-state with a frequency of 1295 cm^{-1} could be assigned (lower left panel, Figure 9). The ethoxy radical and anion photoelectron spectrum have been considered in theoretical treatments by Yarkony and co-workers,[163,164] in which they constructed coupled diabatic states for the two ethoxy states and simulated the photoelectron spectrum. This problem is complicated by a low-lying conical intersection and strong vibronic coupling between the two states; as a result, the energy levels have significant electronic character from both electronic states and their positions are strongly perturbed from a simple harmonic analysis.

Given the considerable effort already expended in analyzing a congested spectrum with partially resolved features, it seemed appropriate to measure a SEVI spectrum of $C_2H_5O^-$ in order to see what new features might be resolved at higher resolution. Preliminary results are shown in the right panel of Figure 9, where we show several scans at increasingly lower photon energies, thereby obtaining progressively narrower energy windows and shifting the region of highest energy resolution toward the band origins. Even the lowest resolution scan is a considerable improvement over the PE spectrum, and the remaining spectra show several new features, including a peak between the band origins and a splitting of peak a, the $\tilde{X}^2A''$ origin, into a doublet spaced by 63 cm^{-1}. These higher resolution spectra will provide a more rigorous test of the theoretical models developed to interpret the data.

B. Probing Prereactive van der Waals Complexes with SEVI. Anion photodetachment has been used in our laboratory and elsewhere to probe transition states for bimolecular and unimolecular reactions.[21,165−168] In these experiments, if a negative ion has good geometric overlap with a reactive transition state, then photodetachment of the anion will access the neutral transition state. Although the transition state is typically short-lived with respect to dissociation to reactants or products,[20] the photoelectron spectrum of the anion in question can yield resolved vibrational structure associated with vibrational motion at the transition state that is perpendicular to the reaction coordinate. As an example, photodetachment of the FH_2^- anion accesses the transition state of the benchmark F + H_2 reaction,[169] yielding resolved progressions in the F−H−H bend and H−H stretch, and thus providing a detailed probe of the potential energy surface in the vicinity of the transition state.[170]

A useful variation of this experiment is when the anion equilibrium geometry does not match the transition state but instead overlaps the shallow van der Waals minimum in either the reactant or product valley of the reaction in question. For example, the ClH_2^- anion has good geometric overlap with the Cl···H_2 van der Waals complex in the reactant valley for the reaction Cl + H_2 → HCl + H.[171,172] Hence, photodetachment of ClH_2^- can, in principle, yield the energy levels of the weakly bound Cl·H_2 complex, providing new insights into a reaction that has played an important role the development of chemical kinetics and dynamics.[173,174] Photodetachment experiments of this type complement infrared studies of "pre-reactive" van der Waals complexes carried out by Lester and co-workers.[175,176]

There are two reasons why the photodetachment of ClH_2^- is of particular interest. First, a study of the Cl + HD reaction by Skouteris et al.[177] provided experimental evidence that the weak van der Waals (vdW) forces in the reactant valley have a significant effect on the branching ratio of the HCl:DCl product as a function of collision energy. These results suggest that spectroscopic study of the prereactive Cl···H_2 complex would provide new insights into how weak vdW interactions affect chemical reactivity. Moreover, such an experiment addresses an ongoing controversy in chemical dynamics concerning the relative reactivities of Cl($^2P_{3/2}$) and

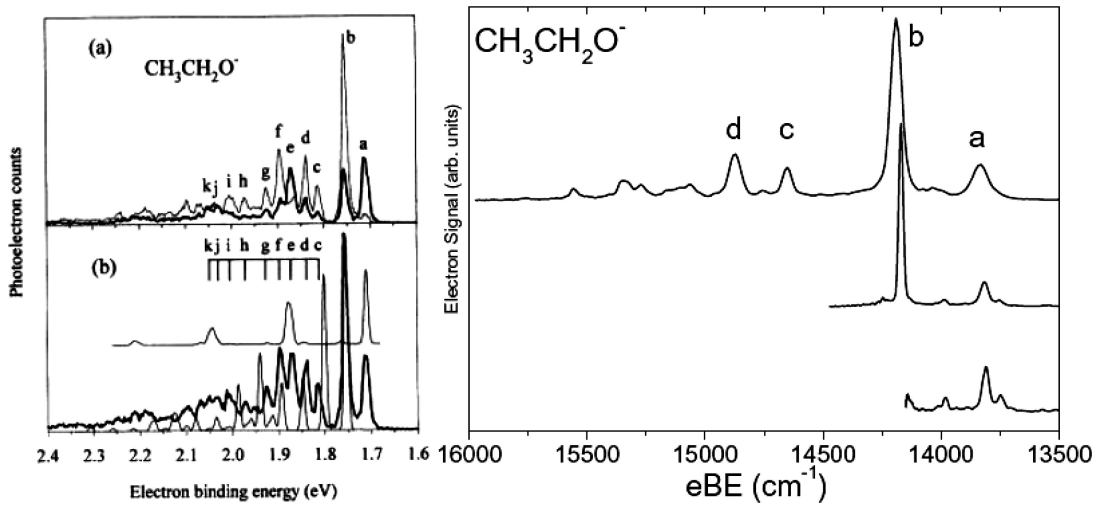

Figure 9. Left: Photoelectron spectra of ethoxide anion from ref 153. Top panel shows results at two different laser polarization angles. Peaks a and b are origins of $\tilde{X}^2A''$ and $\tilde{A}^2A'$ states, respectively. Bottom panel shows "magic angle" spectrum and simulations of transitions to $\tilde{X}$ and $\tilde{A}$ states. Right: SEVI spectra of ethoxide at several photon energies, showing new peaks as the resolution around the two origin peaks is increased.

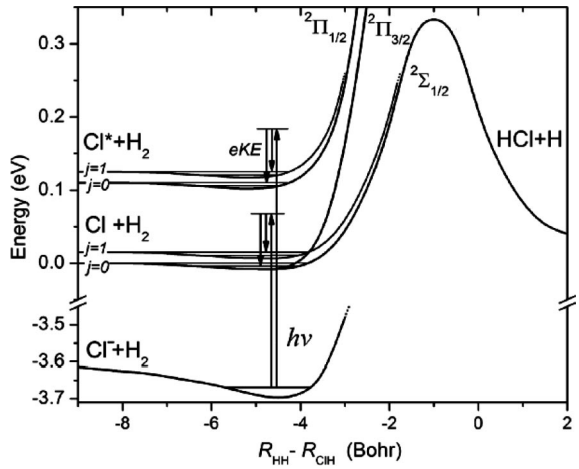

Figure 10. Schematic of adiabatic potential energy curves for $Cl^- + H_2$ and $Cl + H_2$, indicating evolution of $Cl\cdots H_2$ hindered rotor levels to H_2 free rotations and the $Cl\cdots H_2$ van der Waals stretch levels supported by each curve. Note that $Cl^* + H_2$ correlates to electronically excited HCl + H products.

$Cl^*(^2P_{1/2})$ with H_2. As shown in Figure 10, the interaction of Cl and Cl* with H_2 ($^1\Sigma_g^+$) gives rise to three adiabatic electronic PES's, labeled $^2\Sigma_{1/2}$, $^2\Pi_{3/2}$, and $^2\Pi_{1/2}$, in linear geometries. In the adiabatic limit, only $Cl(^2P_{3/2})$ atoms that approach H_2 on the $^2\Sigma_{1/2}$ PES react to form ground-state products. Experience shows that the Born−Oppenheimer (BO) approximation will govern chemical reactions, so that the electronically adiabatic pathway should always dominate. However, experiments by Liu and co-workers[178] indicated that the Cl* state was more reactive than Cl over a wide range of collision energies, a result that disagrees with the BO approximation and with state-of-the-art scattering calculations by Alexander et al.[179] in which nonadiabatic couplings between the reactant spin−orbit states were included. The experimental results thus imply unusually large nonadiabatic effects which, if present, will be strongest in the region of the neutral surface probed by photodetachment of ClH_2^-, where the interaction between the $^2\Sigma$ and $^2\Pi$ states is comparable to the spin−orbit splitting.[180] The photodetachment experiment can therefore probe these effects spectroscopically.

Photoelectron spectra of ClH_2^- and ClD_2^- obtained using a conventional negative ion time-of-flight photoelectron spectrometer have been reported previously.[181] They exhibited features associated with the spin−orbit splitting in the $Cl\cdots H_2$ complex, but no additional structure was resolved because of the limited resolution, around 8−10 meV. Subsequent theoretical work by Alexander and Manolopoulos[180] demonstrated that the ClH_2^- anion wave function has a good FC overlap with the vibrational and hindered rotor states of the neutral $Cl\cdots H_2$ van der Waals complex. In addition, they predicted that with an energy resolution of 1 meV, several features associated with bound and resonance states of this prereactive complex could be resolved. Hence, the higher resolution offered by SEVI was brought to bear on this system.[182]

Figure 11 shows SEVI spectra in the regions of the two spin−orbit states of the $Cl\cdots H_2$ and $Cl\cdots D_2$ complexes. There is considerable structure seen in all four panels that can readily be assigned by comparison with simulations using high quality anion and neutral potential energy surfaces. In the $Cl(^2P_{3/2})\cdots H_2$ spectrum, the observed peaks are associated with the hindered $H_2(j = 0$ and 1) rotor states of the weakly bound $Cl\cdots H_2$ complex on the ground $^2\Sigma_{1/2}$ electronic PES. One quantum of excitation in the $Cl\cdots H_2$ van der Waals stretching vibration (ν_s) is also observed at 30 cm^{-1} above the ($j = 1$, ν_s=0) level. The $Cl(^2P_{3/2})\cdots D_2$ shows two identifiable progressions: the observed transitions are assigned to hindered D_2 rotor modes ($j = 0$, 1, 2) on the $^2\Sigma_{1/2}$ ground electronic state, with a $Cl\cdots D_2$ stretching vibration resolved for the $j = 1$ and 2 levels.

The experimental results in Figure 11 are compared to two sets of simulations: one in which the Born−Oppenheimer approximation is assumed and one in which the nonadiabatic interactions between the Cl/Cl* + H_2 surfaces are included.[183] Although the electronically adiabatic simulations are in reasonable agreement with most features in the measured spectra, there are some clear differences (on the order of 10 cm^{-1}) between several of predicted peak positions and those observed experimentally. The nonadiabatic simulations are only slightly different but result in better agreement with experiment. The most noticeable difference between the two simulations is the reduction, when the nonadiabatic coupling

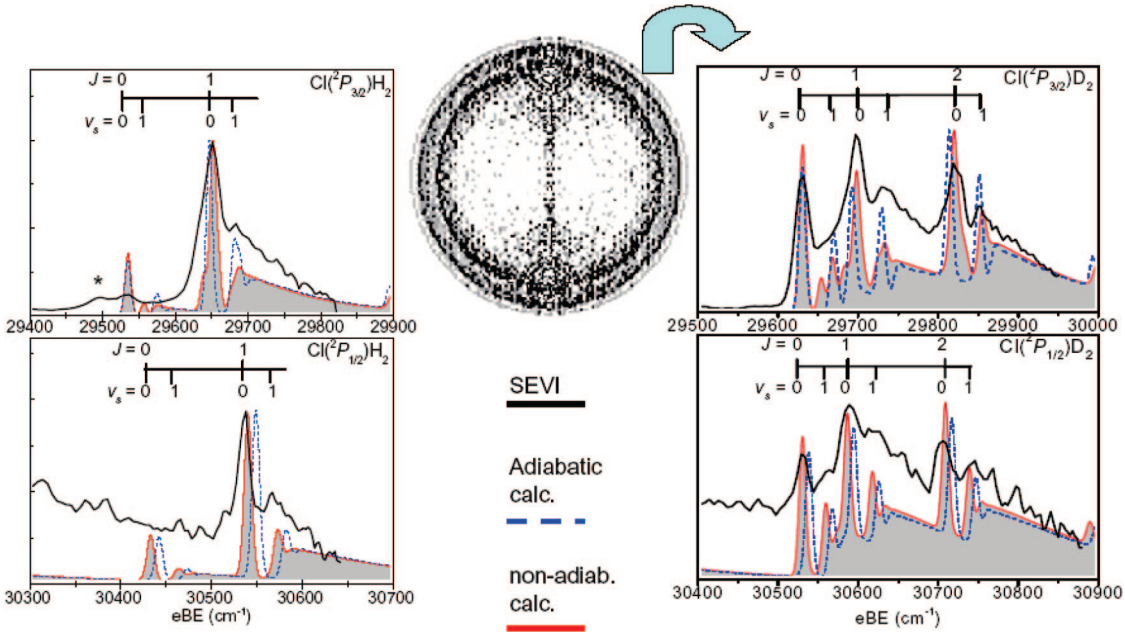

Figure 11. SEVI spectra of ClH_2^- (left) and ClD_2^- (right). Top panels are transitions to $Cl(^2P_{3/2})\cdots H_2$ and $Cl(^2P_{3/2})\cdots D_2$, bottom panels are transitions to $Cl(^2P_{1/2})\cdots H_2$ and $Cl(^2P_{1/2})\cdots D_2$. Spectral assignments are indicated. Results from adiabatic (dashed blue) and nonadiabatic (solid red) simulations are also shown.

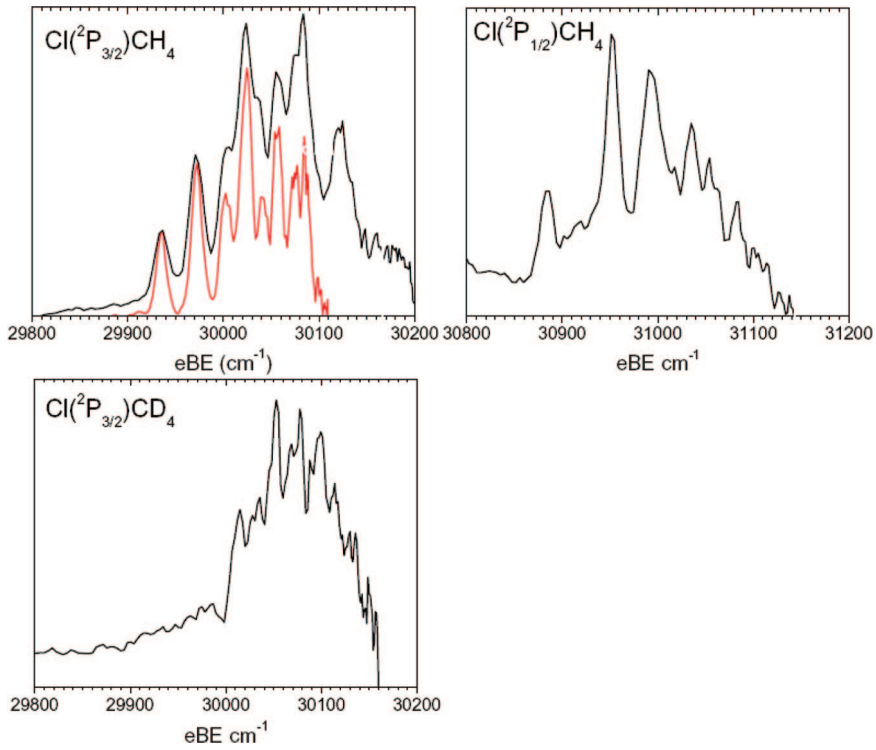

Figure 12. SEVI spectra of $Cl^-(CH_4)$. Top panels, left and right, show transitions to $Cl(^2P_{3/2})\cdots CH_4$ and $Cl(^2P_{1/2})\cdots CH_4$, respectively, while bottom panel shows $Cl(^2P_{3/2})\cdots CD_4$ band.

is retained, of the splitting between the bend−stretch levels associated with the $^2\Sigma_{1/2}$ and $^2\Pi_{1/2}$ states. For example, in the ClH_2 spectra, the splitting between the ($j = 1$, $\nu_s = 0$) levels associated with these two states is reduced from 902 to 888 cm^{-1}, in excellent agreement with the value of 887 cm^{-1} found experimentally. Similarly, in ClD_2, the spacing between the ($j = 0$, $\upsilon_s = 0$) levels is reduced from 908 to 900 cm^{-1} which exactly matches the experimental spectra. These reductions can be explained in terms of small changes in the shapes of the adiabatic-bender potentials induced by the spin−orbit, Coriolis and electrostatic couplings, and the resulting changes in the energies of the bend−stretch van der Waals levels in the two electronic states.

The comparison between experimental and calculated spectra in Figure 11 leads to two important conclusions regarding the Cl + H_2 reaction. First, the level of agreement

of both sets of simulations with the experimental spectra validates the accuracy of the reactant potential energy surfaces in the region of the van der Waals well in the reactant valley. This validation is important because the weak interactions that give rise to this well play a decisive role in determining the product branching ratio of the Cl + HD reaction. Second, these results demonstrate for the first time that the effect of non-Born−Oppenheimer couplings in the prereactive region have been correctly evaluated in the theoretical simulation, to nearly spectroscopic (1 cm^{-1}) accuracy. Calculations at this same level of theory predict nonadiabatic effects in the reaction to be small; the SEVI experiments support this conclusion and suggest a re-examination of the experimental results claiming high reactivity of Cl*.

We have recently performed an analogous experiment on a related polyatomic system, using SEVI of $Cl^-(CH_4)$ to probe the $Cl\cdots CH_4$ prereactive vdW complex for the Cl + CH_4 reaction. The Cl + CH_4 reaction has evolved into a benchmark polyatomic chemical reaction over the last several years that is accessible to detailed experimental and theoretical analysis.[70] The Cl + CH_4 reaction is important in atmospheric ozone chemistry as it controls the Cl/HCl balance in the stratosphere.[184] This reaction has been studied in several laboratories as a model for mode-specific chemistry,[185−189] in which the effect of exciting specific vibrational modes of the CH_4 reactant on the reaction cross section has been investigated and compared to the effect of reactant translational energy.

The anion structure for $Cl-(CH_4)$ has been investigated by Bieske and co-workers[190,191] through a combination of infrared spectroscopy and electronic structure calculations. It is found to have a C_{3v} structure with a linear X−H−C bond in which the Cl^- is bound to the vertex of the CH_4 tetrahedron. The calculated Cl−C bond length in the anion is 3.704 Å. Based on these results, photodetachment of $Cl^-(CH_4)$ should access the prereactive vdW region for the Cl + CH_4 reaction.

We have recently obtained SEVI spectra of $Cl^-(CH_4)$ and $Cl^-(CD_4)$, shown in Figure 12, that show extensive, low-frequency structure. Using the measured association enthalpy of 3.8 kcal/mol for $Cl^-(CH_4)$,[192] and the electron affinity of Cl, we can show that all the vibrational structure in the $Cl-(CH_4)$ SEVI spectrum lies below the Cl + CH_4 asymptote, i.e. it corresponds to bound $Cl\cdots CH_4$ states. By analogy to ClH_2^-,[182] we would expect the $Cl^-(CH_4)$ spectrum to comprise progressions in at least two vibrational modes of the neutral $Cl\cdots CH_4$ complex: hindered rotor motion of the CH_4 and the $Cl\cdots CH_4$ van der Waals stretch. The low-frequency structure is not readily assignable, but the peak spacings are clearly smaller in the $Cl(^2P_{3/2})\cdots CD_4$ band (bottom panel) than in the $Cl(^2P_{3/2})\cdots CH_4$ band. This large isotope effect suggests that there is considerable activity in the hindered rotation of the methane moiety in the spectra.

The low frequency structure in the SEVI spectra reflects the rather complex topology of the reactant Cl + CH_4 reactant valley. In contrast to Cl + H_2, there are three viable minimum energy geometries for van der Waals mimina in the Cl + CH_4 entrance valley with the Cl bound to the vertex, the edge, or the face of the tetrahedron defined by the CH_4 molecule. The first and third bonding motifs have C_{3v} symmetry while the second has C_{2v} symmetry. Calculations of this region of the Cl + CH_4 surface appear to be quite sensitive to the method used: one calculation finds the edge and face structures to be minima, with binding energies of 276 and 348 cm^{-1}, respectively, with a saddle point at the vertex,[193] while another finds more weakly bound minima ($\sim$100 cm^{-1}) at the vertex and face geometries.[194] The SEVI spectra represent the projection of the anion wave function onto the large-amplitude vibrations supported on the neutral surface and can, in principle, distinguish among the possible topologies suggested by the electronic structure calculations. This process will require high level, multidimensional simulations on model potential energy surfaces for the anion and neutral. Efforts are currently underway to collaborate with theory groups in order to carry out these calculations.

IV. Summary and Outlook

The combination of high resolution and versatility offered by SEVI suggests that it will become a powerful new tool in probing reactive free radicals, open-shell complexes, clusters, and transition states by negative ion photodetachment. The results presented in this paper represent the "tip of the iceberg"; studies of many more systems are currently underway in our laboratory.

However, the enhanced capabilities of SEVI compared to more established photoelectron spectroscopic methods bring about a new set of challenges. The low-frequency structure resolved in the SEVI spectra represents large-amplitude, anharmonic nuclear motion that is considerably more difficult to analyze than the high-frequency, nearly harmonic vibrational structure that typically dominates photoelectron spectra, even if only single Born−Oppenheimer potential energy surfaces are involved. The presence of vibronic coupling introduces further complications. The recently measured SEVI spectrum of C_3H^- is an example of the complexity that can arise.[195] We observed an irregular set of transitions from the $\tilde{a}^3A''$ bent state of the anion to the quasi-linear $\tilde{X}^2\Pi$ state of C_3H (both species have slightly lower-lying cyclic isomers). The bent anion state has a relatively low barrier to linearity, around 500 cm^{-1},[196] and the neutral $\tilde{A}^2\Pi$ state exhibits strong Renner−Teller coupling.[197] Simulation of this spectrum thus requires accounting for the combination of large-amplitude bending motion in the anion with vibronic coupling in the neutral and presents a real challenge Efficient methods for calculating both energy levels and wave functions for both the anion and neutral are needed, and the development of these will be greatly facilitated by close collaboration with theory.

On the experimental side, the resolution of SEVI is sufficiently high that it is often in practice limited by the temperature of the anion beam. The free jet source used in the current configuration of our instrument can often achieve ion temperatures below 100 K, but more efficient and systematic cooling schemes would be desirable. There have been significant advances in recent years in trapping and cooling ions to considerably lower temperatures using radio frequency techniques.[198−200] The incorporation of this capability into a SEVI experiment would produce significant benefits.

Acknowledgment. This research is supported by the Air Force Office of Scientific Research under Grant No. F496290−03−10085. D.M.M. thanks Andreas Osterwalder, Matthew Nee, Jia Zhou, Etienne Garand, and Tara Yacovitch for their contributions to this project.

References and Notes

(1) Brehm, B.; Gusinow, M. A.; Hall, J. L. *Phys. Rev. Lett.* **1967**, *19*, 737.

(2) Leopold, D. G.; Ho, J.; Lineberger, W. C. *J. Chem. Phys.* **1987**, *86*, 1715.

(3) Cheshnovsky, O.; Yang, S. H.; Pettiette, C. L.; Craycraft, M. J.; Liu, Y.; Smalley, R. E. *Chem. Phys. Lett.* **1987**, *138*, 119.
(4) Gantefor, G.; Gausa, M.; Meiwesbroer, K. H.; Lutz, H. O. *Faraday Disc.* **1988**, 197.
(5) Handschuh, H.; Cha, C. Y.; Bechthold, P. S.; Gantefor, G.; Eberhardt, W. *J. Chem. Phys.* **1995**, *102*, 6406.
(6) Wu, H. B.; Desai, S. R.; Wang, L. S. *Phys. Rev. Lett.* **1996**, *77*, 2436.
(7) Busani, R.; Folkers, M.; Cheshnovsky, O. *Phys. Rev. Lett.* **1998**, *81*, 3836.
(8) Kostko, O.; Huber, B.; Moseler, M.; von Issendorff, B. *Phys. Rev. Lett.* **2007**, 98.
(9) Markovich, G.; Pollack, S.; Giniger, R.; Cheshnovsky, O. *J. Chem. Phys.* **1994**, *101*, 9344.
(10) Castleman, A. W., Jr.; Bowen, K. H., Jr *J. Phys. Chem.* **1996**, *100*, 12911.
(11) Hendricks, J. H.; Lyapustina, S. A.; Declercq, H. L.; Snodgrass, J. T.; Bowen, K. H. *J. Chem. Phys.* **1996**, *104*, 7788.
(12) Schiedt, J.; Weinkauf, R.; Neumark, D. M.; Schlag, E. W. *Chem. Phys.* **1998**, *239*, 511.
(13) Coe, J. V.; Lee, G. H.; Eaton, J. G.; Arnold, S. T.; Sarkas, H. W.; Bowen, K. H.; Ludewigt, C.; Haberland, H.; Worsnop, D. R. *J. Chem. Phys.* **1990**, *92*, 3980.
(14) Kim, J.; Becker, I.; Cheshnovsky, O.; Johnson, M. A. *Chem. Phys. Lett.* **1998**, *297*, 90.
(15) Verlet, J. R. R.; Bragg, A. E.; Kammrath, A.; Cheshnovsky, O.; Neumark, D. M. *Science* **2005**, *307*, 93.
(16) Lee, G. H.; Arnold, S. T.; Eaton, J. G.; Sarkas, H. W.; Bowen, K. H.; Ludewigt, C.; Haberland, H. *Z. Phys. D* **1991**, *20*, 9.
(17) Lee, I. R.; Lee, W.; Zewail, A. H. *ChemPhysChem* **2008**, *9*, 83.
(18) Mitsui, M.; Nakajima, A.; Kaya, K. *J. Chem. Phys.* **2002**, *117*, 9740.
(19) Mitsui, M.; Ando, N.; Kokubo, S.; Nakajima, A.; Kaya, K. *Phys. Rev. Lett.* **2003**, *91*, 153002.
(20) Polanyi, J. C.; Zewail, A. H. *Acc. Chem. Res.* **1995**, *28*, 119.
(21) Neumark, D. M. *Phys. Chem. Chem. Phys.* **2005**, *7*, 433.
(22) Wang, L. S.; Ding, C. F.; Wang, X. B.; Barlow, S. E. *Rev. Sci. Instrum.* **1999**, *70*, 1957.
(23) Kitsopoulos, T. N.; Waller, I. M.; Loeser, J. G.; Neumark, D. M. *Chem. Phys. Lett.* **1989**, *159*, 300.
(24) Muller-Dethlefs, K.; Sander, M.; Schlag, E. W. *Chem. Phys. Lett.* **1984**, *112*, 291.
(25) Muller-Dethlefs, K.; Schlag, E. W. *Annu. Rev. Phys. Chem.* **1991**, *42*, 109.
(26) Waller, I. M.; Kitsopoulos, T. N.; Neumark, D. M. *J. Phys. Chem.* **1990**, *94*, 2240.
(27) Wetzel, D. M.; Brauman, J. I. *Chem. Rev.* **1987**, *87*, 607.
(28) Osterwalder, A.; Nee, M. J.; Zhou, J.; Neumark, D. M. *J. Chem. Phys.* **2004**, *121*, 6317.
(29) Turner, D. W. *Molecular Photoelectron Spectroscopy*; Wiley: London, 1970.
(30) Berkowitz, J. *Photoabsorption, Photoionization, and Photoelectron Spectroscopy*; Academic Press: New York, 1979.
(31) Siegel, M. W.; Bennett, R. A.; Celotta, R. J.; Hall, J. L.; Levine, J. *Phys. Rev. A* **1972**, *6*, 607.
(32) Kasdan, A.; Herbst, E.; Lineberger, W. C. *J. Chem. Phys.* **1975**, *62*, 541.
(33) Kasdan, A.; Lineberger, W. C. *Phys. Rev. A* **1974**, *10*, 1658.
(34) Feigerle, C. S.; Corderman, R. R.; Bobashev, S. V.; Lineberger, W. C. *J. Chem. Phys.* **1981**, *74*, 1580.
(35) Ervin, K. M.; Lineberger, W. C. *J. Phys. Chem.* **1991**, *95*, 1167.
(36) Breyer, F.; Frey, P.; Hotop, H. *Z. Phys. A* **1981**, *300*, 7.
(37) Oakes, J. M.; Ellison, G. B. *J. Am. Chem. Soc.* **1983**, *105*, 2969.
(38) Snodgrass, J. T.; Coe, J. V.; Freidhoff, C. B.; McHugh, K. M.; Bowen, K. H. *Faraday Discuss.* **1988**, 241.
(39) Bengali, A. A.; Casey, S. M.; Cheng, C. L.; Dick, J. P.; Fenn, P. T.; Villalta, P. W.; Leopold, D. G. *J. Am. Chem. Soc.* **1992**, *114*, 5257.
(40) Rienstra-Kiracofe, J. C.; Tschumper, G. S.; Schaefer, H. F.; Nandi, S.; Ellison, G. B. *Chem. Rev.* **2002**, *102*, 231.
(41) Ervin, K. M.; Ho, J.; Lineberger, W. C. *J. Phys. Chem.* **1988**, *92*, 5405.
(42) Cooper, J.; Zare, R. N. *J. Chem. Phys.* **1968**, *48*, 942.
(43) Reid, K. L. *Annu. Rev. Phys. Chem.* **2003**, *54*, 397.
(44) Johnson, M. A.; Lineberger, W. C. Pulsed methods for cluster ion spectroscopy. In *Techniques of Chemistry*; Farrar, J. M., Saunders, W. H., Jr., Eds.; Wiley Journal: New York, 1988; Vol. 20, pp 591−635.
(45) Posey, L. A.; Deluca, M. J.; Johnson, M. A. *Chem. Phys. Lett.* **1986**, *131*, 170.
(46) Alexander, M. L.; Levinger, N. E.; Johnson, M. A.; Ray, D.; Lineberger, W. C. *J. Chem. Phys.* **1988**, *88*, 6200.
(47) Osborn, D. L.; Leahy, D. J.; Cyr, D. R.; Neumark, D. M. *J. Chem. Phys.* **1996**, *104*, 5026.
(48) Arnold, D. W.; Bradforth, S. E.; Kitsopoulos, T. N.; Neumark, D. M. *J. Chem. Phys.* **1991**, *95*, 8753.
(49) Metz, R. B.; Weaver, A.; Bradforth, S. E.; Kitsopoulos, T. N.; Neumark, D. M. *J. Phys. Chem.* **1990**, *94*, 1377.
(50) Cheshnovsky, O.; Taylor, K. J.; Conceicao, J.; Smalley, R. E. *Phys. Rev. Lett.* **1990**, *64*, 1785.
(51) Yang, J.; Wang, X. B.; Xing, X. P.; Wang, L. S. *J. Chem. Phys.* **2008**, 128.
(52) Kruit, P.; Read, F. H. *J. Phys. E* **1983**, *16*, 313.
(53) Cheshnovsky, O.; Yang, S. H.; Pettiette, C. L.; Craycraft, M. J.; Smalley, R. E. *Rev. Sci. Instrum.* **1987**, *58*, 2131.
(54) Hotop, H.; Lineberger, W. C. *J. Phys. Chem. Ref. Data* **1985**, *14*, 731.
(55) Handschuh, H.; Gantefor, G.; Eberhardt, W. *Rev. Sci. Instrum.* **1995**, *66*, 3838.
(56) Giniger, R.; Hippler, T.; Ronen, S.; Cheshnovsky, O. *Rev. Sci. Instrum.* **2001**, *72*, 2543.
(57) Wang, L.-S.; Cheng, H.-S.; Fan, J. *J. Chem. Phys.* **1995**, *102*, 9480.
(58) Gerhards, M.; Thomas, O. C.; Nilles, J. M.; Zheng, W. J.; Bowen, K. H. *J. Chem. Phys.* **2002**, *116*, 10247.
(59) Baguenard, B.; Pinare, J. C.; Bordas, C.; Broyer, M. *Phys. Rev. A* **2001**, *6302*, 3204.
(60) Baguenard, B.; Pinare, J. C.; Lepine, F.; Bordas, C.; Broyer, M. *Chem. Phys. Lett.* **2002**, *352*, 147.
(61) Surber, E.; Sanov, A. *J. Chem. Phys.* **2002**, *116*, 5921.
(62) Surber, E.; Sanov, A. *Phys. Rev. Lett.* **2003**, *90*, 3001.
(63) Chandler, D. W.; Houston, P. L. *J. Chem. Phys.* **1987**, *87*, 1445.
(64) Heck, A. J. R.; Chandler, D. W. *Annu. Rev. Phys. Chem.* **1995**, *46*, 335.
(65) Helm, H.; Bjerre, N.; Dyer, M. J.; Huestis, D. L.; Saeed, M. *Phys. Rev. Lett.* **1993**, *70*, 3221.
(66) Eppink, A. T. J. B.; Parker, D. H. *Rev. Sci. Instrum.* **1997**, *68*, 3477.
(67) Suzuki, T.; Whitaker, B. J. *Int. Rev. Phys. Chem.* **2001**, *20*, 313.
(68) Stolow, A.; Bragg, A. E.; Neumark, D. M. *Chem. Rev.* **2004**, *104*, 1719.
(69) Ashfold, M. N. R.; Nahler, N. H.; Orr-Ewing, A. J.; Vieuxmaire, O. P. J.; Toomes, R. L.; Kitsopoulos, T. N.; Garcia, I. A.; Chestakov, D. A.; Wu, S. M.; Parker, D. H. *Phys. Chem. Chem. Phys.* **2006**, *8*, 26.
(70) Liu, K. P. *Phys. Chem. Chem. Phys.* **2007**, *9*, 17.
(71) Sanov, A.; Mabbs, R. *Int. Rev. Phys. Chem.* **2008**, *27*, 53.
(72) Suits, A. G. *Acc. Chem. Res.* **2008**, *41*, 873.
(73) Cavanagh, S. J.; Gibson, S. T.; Gale, M. N.; Dedman, C. J.; Roberts, E. H.; Lewis, B. R. *Phys. Rev. A* **2007**, 76.
(74) Gantefor, G. F.; Cox, D. M.; Kaldor, A. *J. Chem. Phys.* **1990**, *93*, 8395.
(75) Bassmann, C.; Boesl, U.; Yang, D.; Drechsler, G.; Schlag, E. W. *Int. J. Mass Spec. Ion Proc* **1996**, *159*, 153.
(76) Distelrath, V.; Boesl, U. *Faraday Disc.* **2000**, *115*, 161.
(77) Lenzer, T.; Yourshaw, I.; Furlanetto, M. R.; Reiser, G.; Neumark, D. M. *J. Chem. Phys.* **1999**, *110*, 9578.
(78) Reiser, G.; Muller-Dethlefs, K. *J. Phys. Chem.* **1992**, *96*, 9.
(79) Chupka, W. A. *J. Chem. Phys.* **1993**, *98*, 4520.
(80) Wigner, E. P. *Phys. Rev.* **1948**, *71*, 1002.
(81) Kitsopoulos, T. N.; Chick, C. J.; Weaver, A.; Neumark, D. M. *J. Chem. Phys.* **1990**, *93*, 6108.
(82) Arnold, C. C.; Neumark, D. M. *J. Chem. Phys.* **1993**, *99*, 3353.
(83) Rohlfing, C. M.; Raghavachari, K. *J. Chem. Phys.* **1992**, *96*, 2114.
(84) Reed, K. J.; Zimmerman, A. H.; Anderson, H. C.; Brauman, J. I. *J. Chem. Phys.* **1976**, *64*, 1368.
(85) Kitsopoulos, T. N.; Chick, C. J.; Zhao, Y.; Neumark, D. M. *J. Chem. Phys.* **1991**, *95*, 5479.
(86) Arnold, C. C.; Zhao, Y. X.; Kitsopoulos, T. N.; Neumark, D. M. *J. Chem. Phys.* **1992**, *97*, 6121.
(87) Kitsopoulos, T. N.; Chick, C. J.; Zhao, Y.; Neumark, D. M. *J. Chem. Phys.* **1991**, *95*, 1441.
(88) Arnold, C. C.; Kitsopoulos, T. N.; Neumark, D. M. *J. Chem. Phys.* **1993**, *99*, 766.
(89) Arnold, C. C.; Neumark, D. M. *J. Chem. Phys.* **1994**, *100*, 1797.
(90) Arnold, C. C.; Xu, C. S.; Burton, G. R.; Neumark, D. M. *J. Chem. Phys.* **1995**, *102*, 6982.
(91) Burton, G. R.; Xu, C. S.; Arnold, C. C.; Neumark, D. M. *J. Chem. Phys.* **1996**, *104*, 2757.
(92) Zhao, Y. X.; Yourshaw, I.; Reiser, G.; Arnold, C. C.; Neumark, D. M. *J. Chem. Phys.* **1994**, *101*, 6538.
(93) Yourshaw, I.; Lenzer, T.; Reiser, G.; Neumark, D. M. *J. Chem. Phys.* **1998**, *109*, 5247.
(94) Wolf, I.; Ronen, S.; Giniger, R.; Cheshnovsky, O. *J. Chem. Phys.* **2005**, 122.
(95) Offerhaus, H. L.; Nicole, C.; Lepine, F.; Bordas, C.; Rosca-Pruna, F.; Vrakking, M. J. J. *Rev. Sci. Instrum.* **2001**, *72*, 3245.

(96) Blondel, C.; Delsart, C.; Dulieu, F. *Phys. Rev. Lett.* **1996**, *77*, 3755.
(97) Delsart, C.; Goldfarb, F.; Blondel, C. *Phys. Rev. Lett.* **2002**, 89.
(98) Zhou, J.; Garand, E.; Neumark, D. M. *J. Chem. Phys.* **2007**, *127*, 114313.
(99) Hansen, E. W.; Law, P. L. *J. Opt. Sci. Am. A* **1985**, *2*, 510.
(100) Xu, C.; Taylor, T. R.; Burton, G. R.; Neumark, D. M. *J. Chem. Phys.* **1998**, *108*, 1395.
(101) Gebhardt, C. R.; Rakitzis, T. P.; Samartzis, P. C.; Ladopoulos, V.; Kitsopoulos, T. N. *Rev. Sci. Instrum.* **2001**, *72*, 3848.
(102) Townsend, D.; Minitti, M. P.; Suits, A. G. *Rev. Sci. Instrum.* **2003**, *74*, 2530.
(103) Ichino, T.; Gianola, A. J.; Lineberger, W. C.; Stanton, J. F. *J. Chem. Phys.* **2006**, 125.
(104) Mahapatra, S.; Cederbaum, L. S.; Koppel, H. *J. Chem. Phys.* **1999**, *111*, 10452.
(105) Chen, P. Photoelectron Spectroscopy of Reactive Intermediates. In *Unimolecular and Bimolecular Ion−Molecule Reaction Dynamics*; Ng, C. Y., Baer, T., Powis, I., Eds.; Wiley: New York, 1994; pp 371−426.
(106) Koppel, H.; Domcke, W.; Cederbaum, L. S. *Adv. Chem. Phys.* **1984**, *57*, 59.
(107) Engelking, P. C.; Lineberger, W. C. *J. Chem. Phys.* **1977**, *67*, 1412.
(108) Ichino, T.; Wren, S. W.; Vogelhuber, K. M.; Gianola, A. J.; Lineberger, W. C.; Stanton, J. F. *J. Chem. Phys.* **2008**, 129.
(109) Weaver, A.; Arnold, D. W.; Bradforth, S. E.; Neumark, D. M. *J. Chem. Phys.* **1991**, *94*, 1740.
(110) Mayer, M.; Cederbaum, L. S.; Koppel, H. *J. Chem. Phys.* **1994**, *100*, 899.
(111) Stanton, J. F. *J. Chem. Phys.* **2007**, 126.
(112) Faraji, S.; Koppel, H.; Eisfeld, W.; Mahapatra, S. *Chem. Phys.* **2008**, *347*, 110.
(113) Mahapatra, S.; Eisfeld, W.; Koppel, H. *Chem. Phys. Lett.* **2007**, *441*, 7.
(114) Asmis, K. R.; Taylor, T. R.; Neumark, D. M. *J. Chem. Phys.* **1999**, *111*, 8838.
(115) Garand, E.; Yacovitch, T. I.; Neumark, D. M. *J. Chem. Phys.* **2008**, 129.
(116) Zengin, V.; Persson, B. J.; Strong, K. M.; Continetti, R. E. *J. Chem. Phys.* **1996**, *105*, 9740.
(117) Choi, H.; Mordaunt, D. H.; Bise, R. T.; Taylor, T. R.; Neumark, D. M. *J. Chem. Phys.* **1998**, *108*, 4070.
(118) Kiefer, J. H.; Sidhu, S. S.; Kern, R. D.; Xie, K.; Chen, H.; Harding, L. B. *Combust. Sci. Technol.* **1992**, *82*, 101.
(119) Guelin, M.; Green, S.; Thaddeus, P. *Astrophys. J.* **1978**, *224*, L27.
(120) Cernicharo, J.; Guelin, M. *Astron. Astrophys.* **1996**, *309*, L27.
(121) McCarthy, M. C.; Gottlieb, C. A.; Gupta, H.; Thaddeus, P. *Astrophys. J.* **2006**, *652*, L141.
(122) Cernicharo, J.; Guelin, M.; Agundez, M.; Kawaguchi, K.; McCarthy, M. C.; Thaddeus, P. *Astron. Astrophys.* **2007**, *467*, L37.
(123) McCarthy, M. C.; Travers, M. J.; Kovacs, A.; Gottlieb, C. A.; Thaddeus, P. *Astrophys. J. Suppl. Ser.* **1997**, *113*, 105.
(124) Gottlieb, C. A.; McCarthy, M. C.; Travers, M. J.; Grabow, J. U.; Thaddeus, P. *J. Chem. Phys.* **1998**, *109*, 5433.
(125) Stephens, J. W.; Yan, W. B.; Richnow, M. L.; Solka, H.; Curl, R. F. *J. Mol. Struct.* **1988**, *190*, 41.
(126) Taylor, T. R.; Xu, C. S.; Neumark, D. M. *J. Chem. Phys.* **1998**, *108*, 10018.
(127) Peric, M.; Peyerimhoff, S. D.; Buenker, R. J. *Z. Phys. D* **1992**, *24*, 177.
(128) Tarroni, R.; Carter, S. *Mol. Phys.* **2004**, *102*, 2167.
(129) Curl, R. F.; Carrick, P. G.; Merer, A. J. *J. Chem. Phys.* **1985**, *82*, 3479.
(130) Christophorou, L. G.; McCorkle, D. L.; Carter, J. G. *J. Chem. Phys.* **1971**, *54*, 253.
(131) Zhou, J.; Garand, E.; Neumark, D. M. *J. Chem. Phys.* **2007**, *127*, 154320.
(132) McCarthy, M. C.; Gottlieb, C. A.; Thaddeus, P.; Horn, M.; Botschwina, P. *J. Chem. Phys.* **1995**, *103*, 7820.
(133) Graf, S.; Geiss, J.; Leutwyler, S. *J. Chem. Phys.* **2001**, *114*, 4542.
(134) Graf, P.; Nitzan, A.; Diercksen, G. H. F. *J. Phys. Chem.* **1996**, *100*, 18916.
(135) Zhou, J.; Garand, E.; Eisfeld, W.; Neumark, D. M. *J. Chem. Phys.* **2007**, 127.
(136) Nee, M. J.; Osterwalder, A.; Zhou, J.; Neumark, D. M. *J. Chem. Phys.* **2006**, *125*, 014306.
(137) Nguyen, T. L.; Mebel, A. M.; Kaiser, R. I. *J. Phys. Chem. A* **2001**, *105*, 3284.
(138) Wheeler, S. E.; Robertson, K. A.; Allen, W. D.; Schaefer, H. F.; Bomble, Y. J.; Stanton, J. F. *J. Phys. Chem. A* **2007**, *111*, 3819.
(139) Goncher, S. J.; Moore, D. T.; Sveum, N. E.; Neumark, D. M. *J. Chem. Phys.* **2008**, *128*, 114303.
(140) Robinson, M. S.; Polak, M. L.; Bierbaum, V. M.; Depuy, C. H.; Lineberger, W. C. *J. Am. Chem. Soc.* **1995**, *117*, 6766.
(141) Eisfeld, W. *Phys. Chem. Chem. Phys.* **2005**, *7*, 3924.
(142) Inoue, G.; Akimoto, H.; Okuda, M. *J. Chem. Phys.* **1980**, *72*, 1769.
(143) Powers, D. E.; Hopkins, J. B.; Smalley, R. E. *J. Phys. Chem.* **1981**, *85*, 2711.
(144) Foster, S. C.; Misra, P.; Lin, T. Y. D.; Damo, C. P.; Carter, C. C.; Miller, T. A. *J. Phys. Chem.* **1988**, *92*, 5914.
(145) Powers, D. E.; Pushkarsky, M. B.; Miller, T. A. *J. Chem. Phys.* **1997**, *106*, 6863.
(146) Lee, Y. Y.; Wann, G. H.; Lee, Y. P. *J. Chem. Phys.* **1993**, *99*, 9465.
(147) Misra, P.; Zhu, X. M.; Hsueh, C. Y.; Halpern, J. B. *Chem. Phys.* **1993**, *178*, 377.
(148) Carrick, P. G.; Brossard, S. D.; Engelking, P. C. *J. Chem. Phys.* **1985**, *83*, 1995.
(149) Geers, A.; Kappert, J.; Temps, F.; Sears, T. J. *J. Chem. Phys.* **1993**, *98*, 4297.
(150) Geers, A.; Kappert, J.; Temps, F.; Wiebrecht, J. W. *J. Chem. Phys.* **1994**, *101*, 3618.
(151) Engelking, P. C.; Ellison, G. B.; Lineberger, W. C. *J. Chem. Phys.* **1978**, *69*, 1826.
(152) Osborn, D. L.; Leahy, D. J.; Kim, E. H.; deBeer, E.; Neumark, D. M. *Chem. Phys. Lett.* **1998**, *292*, 651.
(153) Ramond, T. M.; Davico, G. E.; Schwartz, R. L.; Lineberger, W. C. *J. Chem. Phys.* **2000**, *112*, 1158.
(154) Osborn, D. L.; Leahy, D. J.; Ross, E. M.; Neumark, D. M. *Chem. Phys. Lett.* **1995**, *235*, 484.
(155) Osborn, D. L.; Leahy, D. J.; Neumark, D. M. *J. Phys. Chem. A* **1997**, *101*, 6583.
(156) Barckholtz, T. A.; Miller, T. A. *Int. Rev. Phys. Chem.* **1998**, *17*, 435.
(157) Hoper, U.; Botschwina, P.; Koppel, H. *J. Chem. Phys.* **2000**, *112*, 4132.
(158) Schmidt-Klugmann, J.; Koppel, H.; Schmatz, S.; Botschwina, P. *Chem. Phys. Lett.* **2003**, *369*, 21.
(159) Marenich, A. V.; Boggs, J. E. *Chem. Phys. Lett.* **2005**, *404*, 351.
(160) Gruebele, M.; Roberts, G.; Zewail, A. H. *Phil. Trans. Roy. Soc. London A* **1990**, *332*, 223.
(161) Foster, S. C.; Hsu, Y. C.; Damo, C. P.; Liu, X. M.; Kung, C. Y.; Miller, T. A. *J. Phys. Chem.* **1986**, *90*, 6766.
(162) Curtiss, L. A.; Lucas, D. J.; Pople, J. A. *J. Chem. Phys.* **1995**, *102*, 3292.
(163) Schuurman, M. S.; Young, R. A.; Yarkony, D. R. *Chem. Phys.* **2008**, *347*, 57.
(164) Young, R. A.; Yarkony, D. R. *J. Chem. Phys.* **2006**, 125.
(165) Burnett, S. M.; Stevens, A. E.; Feigerle, C. S.; Lineberger, W. C. *Chem. Phys. Lett.* **1983**, *100*, 124.
(166) de Beer, E.; Kim, E. H.; Neumark, D. M.; Gunion, R. F.; Lineberger, W. C. *J. Phys. Chem.* **1995**, *99*, 13627.
(167) Wenthold, P. G.; Hrovat, D. A.; Borden, W. T.; Lineberger, W. C. *Science* **1996**, *272*, 1456.
(168) Neumark, D. M. *J. Chem. Phys.* **2006**, 125.
(169) Weaver, A.; Metz, R. B.; Bradforth, S. E.; Neumark, D. M. *J. Chem. Phys.* **1990**, *93*, 5352.
(170) Manolopoulos, D. E.; Stark, K.; Werner, H. J.; Arnold, D. W.; Bradforth, S. E.; Neumark, D. M. *Science* **1993**, *262*, 1852.
(171) Wild, D. A.; Weiser, P. S.; Bieske, E. J.; Zehnacker, A. *J. Chem. Phys.* **2001**, *115*, 824.
(172) Bian, W. S.; Werner, H. J. *J. Chem. Phys.* **2000**, *112*, 220.
(173) Alagia, M.; Balucani, N.; Cartechini, L.; Casavecchia, P.; Vankleef, E. H.; Volpi, G. G.; Aoiz, F. J.; Banares, L.; Schwenke, D. W.; Allison, T. C.; Mielke, S. L.; Truhlar, D. G. *Science* **1996**, *273*, 1519.
(174) Alagia, M.; Balucani, N.; Cartechini, L.; Casavecchia, P.; Volpi, G. G.; Aoiz, F. J.; Banares, L.; Allison, T. C.; Mielke, S. L.; Truhlar, D. G. *Phys. Chem. Chem. Phys.* **2000**, *2*, 599.
(175) Wheeler, M. D.; Anderson, D. T.; Lester, M. I. *Int. Rev. Phys. Chem.* **2000**, *19*, 501.
(176) Lester, M. I.; Pond, B. V.; Marshall, M. D.; Anderson, D. T.; Harding, L. B.; Wagner, A. F. *Faraday Disc.* **2001**, *118*, 373.
(177) Skouteris, D.; Manolopoulos, D. E.; Bian, W. S.; Werner, H. J.; Lai, L. H.; Liu, K. P. *Science* **1999**, *286*, 1713.
(178) Dong, F.; Lee, S. H.; Liu, K. *J. Chem. Phys.* **2001**, *115*, 1197.
(179) Alexander, M. H.; Capecchi, G.; Werner, H. J. *Science* **2002**, *296*, 715.
(180) Manolopoulos, D. E.; Alexander, M. H. *Phys. Chem. Chem. Phys.* **2004**, *6*, 4984.
(181) Ferguson, M. J.; Meloni, G.; Gomez, H.; Neumark, D. M. *J. Chem. Phys.* **2002**, *117*, 8181.
(182) Garand, E.; Zhou, J.; Manolopoulos, D. E.; Alexander, M. H.; Neumark, D. M. *Science* **2008**, *319*, 72.
(183) Alexander, M. H.; Klos, J.; Manolopoulos, D. E. *J. Chem. Phys.* **2008**, *128*, 084312.

(184) Solomon, S. *Rev. Geophys.* **1999**, *37*, 275.
(185) Simpson, W. R.; Rakitzis, T. P.; Kandel, S. A.; Orrewing, A. J.; Zare, R. N. *J. Chem. Phys.* **1995**, *103*, 7313.
(186) Yoon, S.; Henton, S.; Zivkovic, A. N.; Crim, F. F. *J. Chem. Phys.* **2002**, *116*, 10744.
(187) Bechtel, H. A.; Camden, J. P.; Brown, D. J. A.; Martin, M. R.; Zare, R. N.; Vodopyanov, K. *Angew. Chem., Int. Ed.* **2005**, *44*, 2382.
(188) Yan, S.; Wu, Y. T.; Zhang, B. L.; Yue, X. F.; Liu, K. P. *Science* **2007**, *316*, 1723.
(189) Espinosa-Garcia, J. *J. Phys. Chem. A* **2007**, *111*, 9654.
(190) Wild, D. A.; Loh, Z. M.; Wolynec, P. P.; Weiser, P. S.; Bieske, E. J. *Chem. Phys. Lett.* **2000**, *332*, 531.
(191) Loh, Z. M.; Wilson, R. L.; Wild, D. A.; Bieske, E. J.; Gordon, M. S. *Aust. J. Chem.* **2004**, *57*, 1157.
(192) Hiraoka, K.; Mizuno, T.; Iino, T.; Eguchi, D.; Yamabe, S. *J. Phys. Chem. A* **2001**, *105*, 4887.
(193) Klos, J. *Chem. Phys. Lett.* **2002**, *359*, 309.
(194) Troya, D.; Weiss, P. J. E. *J. Chem. Phys.* **2006**, 124.
(195) Sheehan, S. M.; Parsons, B. F.; Zhou, J.; Garand, E.; Yen, T. A.; Moore, D. T.; Neumark, D. M. *J. Chem. Phys.* **2008**, *128*, 034301.
(196) Pachkov, M.; Pino, T.; Tulej, M.; Maier, J. P. *Mol. Phys.* **2001**, *99*, 1397.
(197) Peric, M.; Mladenovic, M.; Tomic, K.; Marian, C. M. *J. Chem. Phys.* **2003**, *118*, 4444.
(198) Gerlich, D. *Adv. Chem. Phys.* **1992**, *82*, 1.
(199) Asmis, K. R.; Brummer, M.; Kaposta, C.; Santambrogio, G.; von Helden, G.; Meijer, G.; Rademann, K.; Woste, L. *Phys. Chem. Chem. Phys.* **2002**, *4*, 1101.
(200) Wang, X. B.; Woo, H. K.; Wang, L. S.; Minofar, B.; Jungwirth, P. *J. Phys. Chem. A* **2006**, *110*, 5047.

JP807182Q